

RESEARCH PAPER



## *In vitro* exposure to *Hymenoptera* venom and constituents activates discrete ionotropic pathways in mast cells

C. Jansen<sup>a</sup>, L. M.N. Shimoda<sup>a</sup>, J. Starkus<sup>a</sup>, I. Lange<sup>b</sup>, N. Rysavy<sup>a</sup>, K. Maaetoft-Udsen<sup>a</sup>, C. Tobita<sup>a</sup>, A.J. Stokes <sup>c</sup>, and H Turner<sup>a</sup>

<sup>a</sup>Laboratory of Immunology and Signal Transduction, Division of Natural Sciences and Mathematics, Chaminade University, Honolulu, Hawai'i, USA; <sup>b</sup>Department of Pharmaceutical Sciences, Daniel K. Inouye College of Pharmacy, University of Hawai'i at Hilo, Hilo, Hawai'i, USA; <sup>c</sup>Department of Cell and Molecular Biology, Laboratory of Experimental Medicine, John A. Burns School of Medicine, University of Hawai'i, Honolulu, Hawai'i, USA

### ABSTRACT

Calcium entry is central to the functional processes in mast cells and basophils that contribute to the induction and maintenance of inflammatory responses. Mast cells and basophils express an array of calcium channels, which mediate responses to diverse stimuli triggered by small bioactive molecules, physicochemical stimuli and immunological inputs including antigens and direct immune cell interactions. These cells are also highly responsive to certain venoms (such as *Hymenoptera* envenomations), which cause histamine secretion, cytokine release and an array of pro-inflammatory functional responses. There are gaps in our understanding of the coupling of venom exposure to specific signaling pathways such as activation of calcium channels. In the present study, we performed a current survey of a model mast cell line selected for its pleiotropic responsiveness to multiple pro-inflammatory inputs. As a heterogenous stimulus, *Hymenoptera* venom activates multiple classes of conductance at the population level but tend to lead to the measurement of only one type of conductance per cell, despite the cell co-expressing multiple channel types. The data show that  $I_{CRAC}$ ,  $I_{ARC}$ , and TRPV-like currents are present in the model mast cell populations and respond to venom exposure. We further assessed individual venom components, specifically secretagogues and arachidonic acid, and identified the conductances associated with these stimuli in mast cells. Single-cell calcium assays and immunofluorescence analysis show that there is heterogeneity of channel expression across the cell population, but this heterogeneity does not explain the apparent selectivity for specific channels in response to exposure to venom as a composite stimulus.

### ARTICLE HISTORY

Received 30 May 2019  
Revised xx xxx xxxx  
Accepted 31 May 2019

### KEYWORDS

Mast cells; calcium; bee venom; allergy

## Introduction

Calcium is a central second messenger to a plethora of biological processes [1]. Calcium entry in mast cells and basophils regulates cytokine gene transcription, secretory granule exocytosis, and other functional responses [2]. Calcium fluxes across the plasma membrane in mast cells and basophils are conveyed by a markedly diverse set of calcium channels, including calcium release activated calcium (CRAC) channels, arachidonic acid-activated channels (ARC), various transient receptor potential (TRP) channels of the C (canonical), M (Melastatin-like), and V (Vanilloid) sub-families. KIR, KCa as well as all of the different Kv potassium channels have also been reported in mast cells and basophils [3]. These support calcium entry through modulating driving force (membrane potential) in a receptor-

driven and immunologically responsive manner [4]. With so many parallelized calcium entry pathways across the PM, cells clearly have the potential to respond to diverse single inputs.

Stimuli that induce calcium mobilization in mast cells and basophils include immunological stimuli (innate and adaptive immune pathways including Toll-like Receptors (TLR) and high-affinity receptor for IgE (FcεRI) and Fcγ receptor signaling). Physical and mechanical stimuli, and potent small molecules from diverse chemical families (including arachidonic acid, various plant-derived and other environmental stimuli, etc.) also activate mast cells and basophils. *Hymenoptera* venoms are potent activators of mast cells and basophils, inducing secretory granule exocytosis and histamine release. Envenomation sites display

**CONTACT** H Turner  [hturner@chaminade.edu](mailto:hturner@chaminade.edu)

*rubor, calor, dolor, and tumor* [5], primarily orchestrated by the release of factors that induce inflammation, activate sensory neurons, increase vascular permeability and recruit other leukocytes using chemokine gradients. The components of venoms are incompletely understood (no complete proteome and metabolome have yet been published), but the classes of mediator that they contain include antigens, peptide and small-molecule secretagogues, and soluble phospholipase A2 (which generates arachidonic acid at the plasma membrane). Example published compositions of venoms include a cocktail of many proteins and enzymes, which include hyaluronidase, phospholipases (PLA) A1 and A2, mellitin, mastoparans, apamine, mast cell degranulating peptide, histamine, adolapin, oligopeptides, phospholipids, saccharides, acid phosphatase, and histamine [6]. Clearly, venoms are a complex, multi-component, stimulus that, when impacting the mast cell or basophil membrane, would have several co-incident mechanisms to activate multiple calcium entry pathways in parallel. The current study has two motivations. First, bee venoms are associated with human pathology ranging from irritation to anaphylaxis, and ion channels activated by the venoms are intrinsically targets for possible intervention. However, in order to intervene, it is necessary to know which ion channels should be targeted and are relevant to envenomation. Conversely, bee venoms and their components are being proposed as therapies in diverse disorders [7]. Again, an understanding of their mechanisms of action is critical to predicting therapeutic modality and potential side effect profiles. One of the motivations for the current study is, therefore, the identification of the specific ionotropic responses initiated by bee venom in a model mast cells. Second, in the  $\text{Ca}^{2+}$  signaling field, stimuli that couple to ion channels tend to be studied unilaterally and in isolation. Perhaps less well-understood are the pathways and impact of co-incident stimuli that could potentially activate multiple calcium entry routes simultaneously, an example of which would be *Hymenoptera* envenomation.

In the current study, we dissected the calcium responses to venom and examples of its components, with a particular interest in assessing whether

disparate calcium entry pathways were simultaneously activated or whether individual pathways took precedence. Three entry pathways were the focus of this study, although there is undoubtedly more diversity of channel expression in these cells [8–12].

First, calcium release activated calcium (CRAC) currents were first described in the early 1990s in mast cells and chromaffin cells [13]. The molecular identity for  $I_{\text{CRAC}}$  is a hexamer of ORAI1 subunits [14,15]. CRAC channels are highly calcium selective and are inhibited by Lanthanum and 2-Aminoethoxydiphenyl borate (2-APB) [16]. CRAC channels are activated by endoplasmic reticulum (ER) calcium store depletion, which leads to store-operated calcium entry (SOCE). The activation of CRAC channels occurs when stromal interaction molecule 1 (STIM1), a calcium sensor in the ER, moves to the membrane and directly activates ORAI1 channels [17,18]. CRAC channel current-voltage relationships show a high level of inward rectification and reverse near +60 mV.

Second, Transient Receptor Potential Vanilloid channels (TRPV family) are nonselective cation channels that are largely associated with pain sensation [19], and a number of the family members are expressed in mast cells. TRPVs in mast cells respond to further physicochemical stimuli and a range of small molecules. For example, TRPV1 is activated by capsaicin, heat, anandamide, and exogenous cannabinoids [20]. Activation of TRPV1 by the venom peptide mellitin [21,22] has been described for TRPV1 in sensory neurons but not in mast cells [23,24]. TRPV1 is permeable to the cations sodium, lithium, potassium, cesium, calcium, and magnesium [25], and is not inhibited by Lanthanum or 2-APB. The current-voltage relationship for TRPV1 shows an outwardly rectifying current that reverses near 0 mV.

Third, arachidonic acid-regulated channels (ARC) are also a source of calcium entry into the mast cells [26,27]. ARC channels share similar biophysical characteristics with CRAC channels in that ARC channels are highly selective for calcium and have small conductances similar to CRAC channels. ARC is composed of ORAI1 and ORAI3 subunits [28]. The ARC current-

voltage relationship is very similar to CRAC channels, showing positive reverse potential near +60 mV and a high inward rectification [29]. Differentiation between ARC and CRAC requires analysis of sensitivity to the CRAC (but not ARC) inhibitor 2-APB.

In the current study, we exposed a model mast cell line to venoms, and individual venom components or products. We sought to assess the impact of complex venoms on activation of calcium entry pathways to understand further the decoding of these multi-component stimuli and to identify the calcium entry mechanisms that would hold subsequent importance for understanding venom pathology and outcomes/mechanism of therapeutic venom exposure [30]. We performed a current survey focusing on these three calcium entry mechanisms of a model mast cell line selected for its pleiotropic responsiveness to multiple pro-inflammatory inputs. The data show that  $I_{\text{CRAC}}$ ,  $I_{\text{ARC}}$ , and TRPV conductances are present in model mast cell populations, but at varying frequencies and abundancies, and responding to diverse single stimuli. *Hymenoptera* venom acts as a composite stimulus and activates multiple classes of conductance at the population level but tend to lead to the induction of only one type of conductance per cell.

## Methods

### Cell culture

RBL2H3 [31] were grown at 37°C, 5% CO<sub>2</sub>, in 95% humidity in Dulbecco's Modification of Eagle Medium (Mediatech Inc., Herndon, VA) with 10% heat-inactivated Fetal Bovine Serum (Mediatech) and 2 mM L-glutamine. HEK TRexTRPV1 were cultured in DMEM, 10% Fetal Bovine Serum, 2 mM L-glutamine, 10 µg/ml Blasticidin (Calbiochem, San Diego CA), 400 µg/ml Zeocin (InvivoGen, San Diego CA), transgene expression was induced using 1 µg/ml Tetracycline for 16–24 h.

### Chemicals, reagents, and stimulations

General chemicals were from VWR (West Chester, PA) and Sigma Aldrich (St. Louis, MO). Phorbol myristate acetate (PMA) and Ionomycin were from Calbiochem (Gibbstown, NJ). IgE anti-DNP is from Sigma and KLH-

DNP was from Calbiochem. Bee venom was from HollisterStier (Spokane, WA). To mitigate batch-to-batch variation in venom, three independent batches were selected on the basis of similar potency for induction of histamine release in control experiments, mixed, aliquoted and used for the duration of the studies presented here. Mastoparan and Mellitin were from Sigma Aldrich. Arachidonic acid was from Enzo (Farmingdale, NY). 2-Aminoethoxydiphenyl borate (2-APB) was from Calbiochem (La Jolla, CA). Capsaicin and Capsazepine were from Sigma Aldrich. FcεRI stimulation used 0.1 µg/ml IgE anti-DNP for 16 h at 37°C, followed by three washes and the addition of 250 ng/ml KLH-DNP for the indicated times. PMA and ionomycin were both used at 500 nM. Arachidonic acid and other stimuli were used at concentrations specified in the Figure legends. Antibodies were obtained as follows: ORAI1: rabbit polyclonal (Abcam, Cambridge, UK), mouse monoclonal (ThermoFisher, Waltham, MA); ORAI3, rabbit polyclonal (Abcam), mouse monoclonal (ThermoFisher); TRPV1, rabbit polyclonal AJS/HT, mouse monoclonal BS397 (Abcam); TRPV2 rabbit polyclonal AJS/HT, anti-TRPV2-FITC rabbit polyclonal directly conjugated (Alomone); TRPA1 rabbit polyclonal (AJS, Bethyl; Laboratories), mouse monoclonal (Abnova). Secondary antibodies were Alexa-488 or 568 goat anti-rabbit or rabbit anti-mouse (Molecular Probes, Eugene, OR).

### Mast cell degranulation assay

RBL2H3 were plated in 48 well cluster plates at  $5 \times 10^4$  cells/well. Cells were primed for 16 h at 37°C with 1 µg/ml IgE anti-dinitrophenol (DNP, Sigma, St Louis, MI). Monolayers were washed and incubated in 200 µl Tyrode's buffer before stimulating as described in the Figure legend. After 45 min at 37°C, 25 µl supernatant was removed, clarified by microcentrifugation, and transferred to a 96-well plate containing 100 µl per well PNAG substrate solution (1 mM p-N-acetyl glucosamine (Sigma) in 0.05 M citrate buffer pH 4.5). After 1 h at 37°C, reactions were quenched by the addition of 100 µl per well 0.2 M glycine, pH 9.0. Beta-hexosaminidase levels were read as OD at 405

nm. Results are shown as the mean  $\pm$  standard deviation.

### **Calcium assay (bulk method)**

RBL2H3 were washed and incubated with 0.2  $\mu$ M Fluo-4 [32] for 30 min at 37°C in a modified Ringer's solution of the following composition (in mM): NaCl 145, KCl 2.8, CsCl 10, CaCl<sub>2</sub> 10, MgCl<sub>2</sub> 2, glucose 10, Hepes-NaOH 10, pH 7.4, 330 mOsm. Nominally calcium-free conditions were generated by omitting CaCl<sub>2</sub> and adding 2mM EGTA. Cells were transferred to 96-well plates at 100,000 cells/well and stimulated as indicated. Calcium signals were acquired using a Flexstation 3 (Molecular Devices, Sunnydale, USA). Data were analyzed using SoftMax<sup>®</sup> Pro 5 (Molecular Devices). Where indicated, nominally calcium-free external conditions were achieved by the preparation of 0 mM CaCl<sub>2</sub> Ringer solution containing 1 mM EGTA.

### **Calcium assay (single cell method)**

RBL2H3 were plated on glass coverslip dishes (MatTek, Ashland, MA) and incubated with 1  $\mu$ M Fluo-4 for 30 min at 37°C in modified Ringer's solutions as described above. After washing, cells were stimulated as indicated on a 37°C heated stage. Calcium signals were acquired using a Nikon Ti Eclipse confocal microscopy system, using EZ C1 software for acquisition and NIS Elements software (Nikon) for analysis. Where indicated, nominally calcium-free external conditions were achieved by the preparation of 0 mM added CaCl<sub>2</sub> Ringer solution containing 1 mM EGTA.

### **Electrophysiology**

Cells grown on glass coverslips were transferred to the recording chamber and kept in a standard-modified Ringer's solution. For the experiments measuring  $I_{CRAC}$  and  $I_{ARC}$  like currents a standard-modified Ringer's external solution of the following composition was selected (in mM): NaCl 120, CaCl<sub>2</sub> 20, MgCl<sub>2</sub> 2, CsCl 10, glucose 10, Hepes-NaOH 10, pH 7.2, with osmolarity typically ranging from 295 to 325 mOsm. Intracellular pipette-filling solutions contained (in mM): Cs-glutamate 120, MgCl<sub>2</sub> 1, CaCl 4, Cs-BAPTA 10,

HEPES-CsOH 10, pH 7.2 adjusted with CsOH with a free calcium concentration of 150 nM. The external solutions used with the TRPV1 over-expressing HEK cells contained: NaCl 140, KCl 2.8, CaCl<sub>2</sub> 1, MgCl<sub>2</sub> 2, Hepes-NaOH 10. The internal solution used with TRPV1 overexpressing HEK cells contained: Cs-glutamate 120, Cs Bapta 10, CaCl<sub>2</sub> 4.1, MgCl<sub>2</sub> 1, NaCl 8, HEPES-CsOH 10, pH 7.3 and osmolarity around 300 mOsm. The internal solution contained 150 nM free calcium. Patch-clamp experiments were performed in the tight-seal whole-cell configuration at 21–25°C. High-resolution current recordings were acquired by a computer-based patch-clamp amplifier system (EPC-10-USB, HEKA, Lambrecht, Germany). Patch pipettes had resistances between 2 and 4 M $\Omega$  after filling with the standard intracellular solution. Immediately following the establishment of the whole-cell configuration, voltage ramps of 50 ms duration spanning the voltage range of –100 to +100 mV were delivered from a holding potential of 0 mV at a rate of 0.5 Hz over a period of 500 s. All voltages were corrected for a liquid junction potential of 10 mV between external and internal solutions because of glutamate use as an intracellular anion. Currents were filtered at 2.9 kHz and digitized at 100  $\mu$ s intervals. Capacitive currents and series resistance were determined and corrected before each voltage ramp using the automatic capacitance compensation of the EPC-10-USB. The current development graphs were generated by extracting currents at –80 mV and +80 mV. Where applicable, statistical errors of averaged data are given as means  $\pm$  SEM with n determinations. Trace subtraction was performed on small calcium currents to measure  $I_{CRAC}$  and  $I_{ARC}$  like currents. A stable trace was selected and subtracted from all of the traces, which removes the current recorded prior to application leaving only current that develops after application of the compounds. If internal solution application was used, the earliest stable trace was selected for subtraction.

### **Imaging**

Immunofluorescence staining was carried out as follows: Cells were seeded on glass coverslips and transferred to 24-well cluster plates for staining.

Fixation was with methanol (1 min). Blocking was with 5% (v/v) fish skin gelatin (FSG) for 15 min at RT. Primary antibodies were applied singly or in combination in PBS 0.1% (v/v) FSG for 1 h. After three washes in PBS, secondary antibodies were applied at 0.1  $\mu\text{g}/\text{ml}$  for 30 min in PBS 0.1% (v/v) FSG. After three washes in PBS, coverslips were dipped in  $\text{dH}_2\text{O}$  and mounted in Crystal Mount (Electron Microscopy Services). Secondary-alone coverslips were prepared with a sham exposure (no primary antibody exposure), but all other steps in the protocol unchanged. Bright field and fluorescence imaging of cells were performed on a Nikon Ti Eclipse C1 epi-fluorescence and confocal microscopy system. Images were analyzed in NIS Elements (Nikon, Melville, NY). Unless otherwise stated, images were acquired through a Plan Apo VC  $100\times 1.40$  oil objective (Nikon).

### Analysis

Results are shown as the mean  $\pm$  standard deviation. Statistical significance was determined based on Student's t-test or ANOVA. Adjacent to data points in the respective graphs, significant differences were recorded as follows: single asterisk,

$p < 0.05$ ; double asterisk,  $p < 0.01$ ; triple asterisk,  $p < 0.001$ ; no symbol,  $p > 0.05$ . Experiments are all  $n$  of at least 3.

## Results

### *Bee and wasp venoms differentially induce functional responses in model mast cells*

Bee and wasp venoms both activate mast cell-driven inflammatory responses. Both contain potentially ionotropic and calcium-mobilizing stimuli which contain numerous components including peptide antigens, secretagogues, arachidonate-generating enzymes, and small molecules. We identified sources of both venoms and obtained multiple batches that were then mixed and aliquotted to provide long-term consistency across the experiments presented in this study. We initially screened doses of bee and wasp venoms for the ability to induce degranulation in the model mast cell line selected for this study (Figure 1). Our dose-response analysis showed that lytic events are uncommon (trypan blue positivity after 30  $\mu\text{g}/\text{ml}$  venom exposure for 25 min  $<15\%$  in both venoms), and that secretory events are

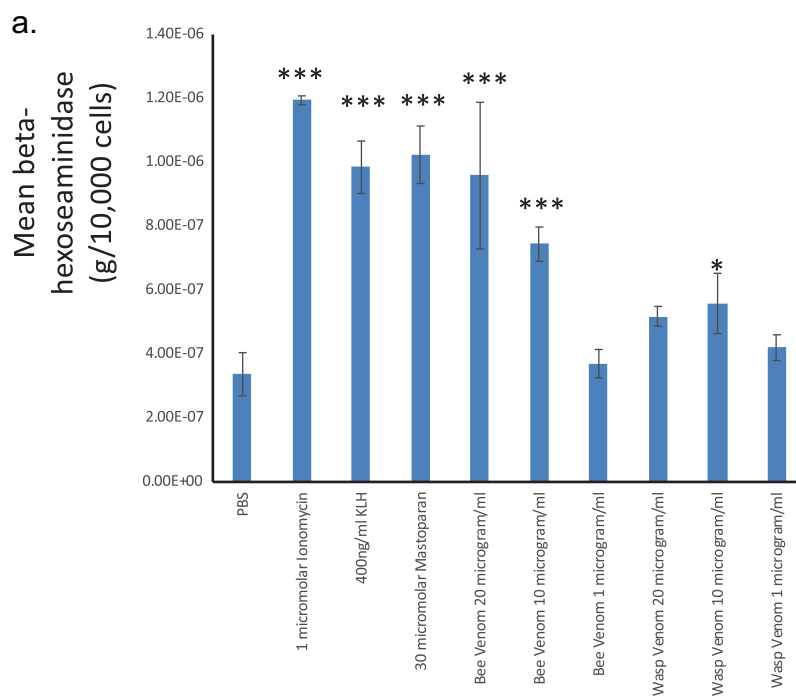


**Figure 1.** (a) Beta-hexosaminidase release from RBL2H3. RBL2H3 were stimulated for 60 min with the indicated agents and levels of beta-hexosaminidase secreted into the extracellular milieu were assayed using a colorimetric protocol. Data are presented as standard errors around a mean of triplicate samples, and significant (Student's t-test) differences from non-stimulated (NS) controls are denoted by asterisks.

observed in response to both venoms. **Figure 1** shows a beta-hexosaminidase assay (a proxy for histamine release), which was performed on the RBL2H3 cells after 30 min of stimulation by both wasp venom and bee venom. Both venoms showed the release of beta-hexosaminidase in a dose-dependent manner. The lower potency of wasp venom was noted and in subsequent experiments, we focused on bee venom. The wasp venom showed a level of histamine release that was lower than the mastoparan, a secretagogue peptide in wasp venom, as well as ionomycin. The bee venom showed a dose-dependent increase in histamine release that approached that achieved through ionomycin.

### **Bee venom initiates $Ca^{2+}$ entry and diverse $Ca^{2+}$ -permeant conductances in mast cells**

We applied bee venom (BV) to the RBL2H3 mast cell and measured both  $Ca^{2+}$  influx and the resulting conductances. **Figure 2(a)** shows that BV induces a large mobilization of intracellular  $Ca^{2+}$ . **Figure 2(b)** dissects this response into the release from intracellular stores and influx. Cells were stimulated in a nominally calcium-free Ringer solution (0 mM additional  $CaCl_2$  plus 2 mM EGTA). Under these conditions, any calcium fluxes observed come from intracellular store depletion. At 100 s, extracellular calcium levels are restored to 1 mM, and any channels that have been opened either in response to store depletion or due to direct channel activation of non-store-operated channels, manifest as a large influx signal. We note that bee venom induces some store release and activates a large influx response.

The whole-cell patch-clamp technique was used to further investigate the effects of bee venom at the single-cell level in RBL2H3 cells. We performed a current survey where RBL2H3 cells were assayed in the whole-cell patch-clamp configuration and once the current-stabilized venom was applied. Across the cell population, we noted that different cells exhibited distinct conductances in response to this treatment. We preliminarily categorized these currents into three types – types A, B, and C. Type A, B, and C currents occurred in 50%, 33%, and 17% of the cells examined, respectively. The leak subtracted type A current (**Figure 2(c,f,i)**, red

traces) stabilized after a few seconds and took about 500 s of bee venom application for current to activate. The type A current resulting from bee venom application is inward rectifying with a positive reverse potential. The Type A inward current at  $-80$  mV showed on average 1 pA/pF current density. The leak subtracted type B current (**Figure 2(d,g,j)** blue traces) also stabilized after a few seconds, but the inward current appeared to activate faster at about 300 s as well as a contained a small outward component that inactivates over the 600 s. The current-voltage relationship for Type B shows a similar inward rectification as Type A but also contains a further positively shifted reverse potential. The type B current density measured at  $-80$  mV showed on average around 1.2 pA/pF. The type C (**Figure 2(e,h,k)** black traces) current developed after 200 s of bee venom application and was much larger than the type A and type B currents. The type C current-voltage relationship shows an outwardly rectifying current that ends as a linear current with  $\sim 650$  pA/pF of inward and outward current. The outward current developed more slowly than the inward current.

### **The diverse venom-induced conductances can be attributed to $I_{ARC}$ , $I_{CRAC}$ and TRPV1**

We sought to identify the ion channel supporting each of the Type A, B, and C conductances. Initially, we focused on Type A and B currents, which we hypothesized to be CRAC or ARC, which require some pharmacological approaches to differentiate them. Both have positive reversal potentials but CRAC is sensitive to 2-APB inhibition while ARC is not, a property that we used to differentiate them. The type A current which shows a  $\sim +70$  mV reverse potential and inward rectification was allowed to develop and then 50  $\mu$ M 2-APB was applied to the Type A current. The 50  $\mu$ M 2-APB application inhibited the type A current (**Figure 3(a–c)**). The Type B current did not show 2-APB inhibition (**Figure 3(g,h,i)**). Intracellular inositol (1,4,5) triphosphate (IP3) and extracellular arachidonic acid were applied to provide positive control recordings for CRAC and ARC, respectively (**Figure 3(d,e,f,j,k,l)**). The IP3 induced CRAC currents showed an inward

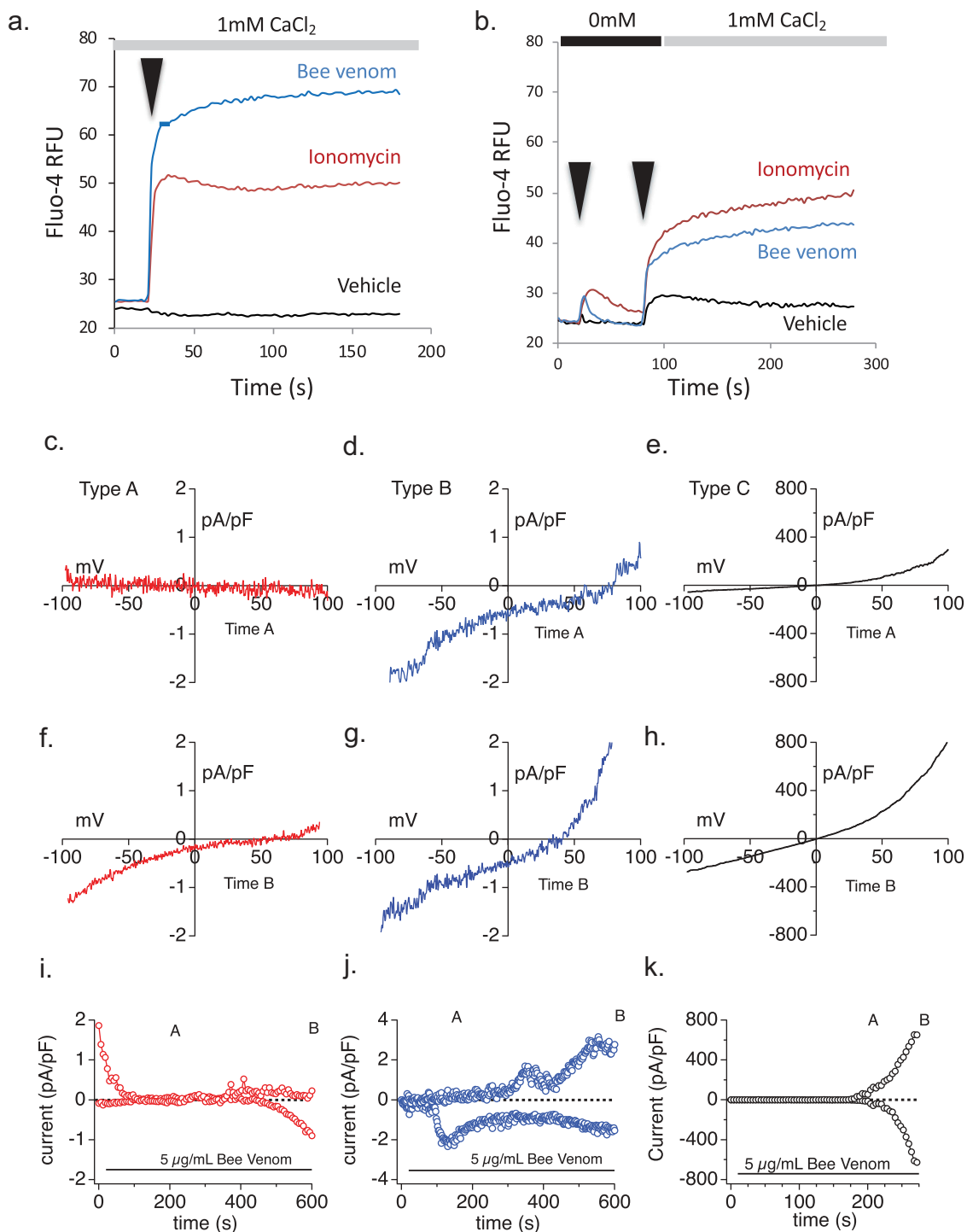


**Figure 2.** Venom-induced Ca<sup>2+</sup> responses and conductances in RBL2H3. (a,b) Population-based calcium assays of RBL2H3 responses to venom and venom-associated stimuli in the presence and absence of external calcium. Fluo-4-AM was used to load RBL2H3 in a modified Ringer's solution containing 1 mM external CaCl<sub>2</sub>. Experimental readings were carried out either in 1 mM external CaCl<sub>2</sub> (a) or in 0 mM CaCl<sub>2</sub> with 1 mM EGTA followed by re-addition of CaCl<sub>2</sub> to a concentration of 1 mM final (b). Cells were stimulated after a period of establishing baseline (usually 20 s) by addition of vehicle (matched diluent to each stimulus), Ionomycin (500 nM), or Bee Venom (5 µg/ml). (c–k) Bee venom current survey. (c,f,i) Type A representative current-voltage relationships taken after background subtraction at indicated time points (see current development graph in 2 I) of 5 µg/ml bee venom application. The data in Figures (c,f,i) were all recorded from the same RBL2H3 cell (red). (d,g,j) Type B current-voltage relationship taken after background subtraction at indicated time points (see current development graph in 2 J) of 5 µg/ml bee venom application. The data in Figure 2(d,g,j) were all recorded from the same RBL2H3 cell (blue). (e,h,k) Type C current-voltage relationships taken at indicated time points (see current development graph in 2 K) of 5 µg/ml bee venom application. The data in Figure 2(e,h,k) were all recorded from the same RBL2H3 cell (black). Note that application times were the same for each figure, but the extraction point for I/V curves may vary. The current development graphs were generated by extracting currents at –80 mV and +80 mV.

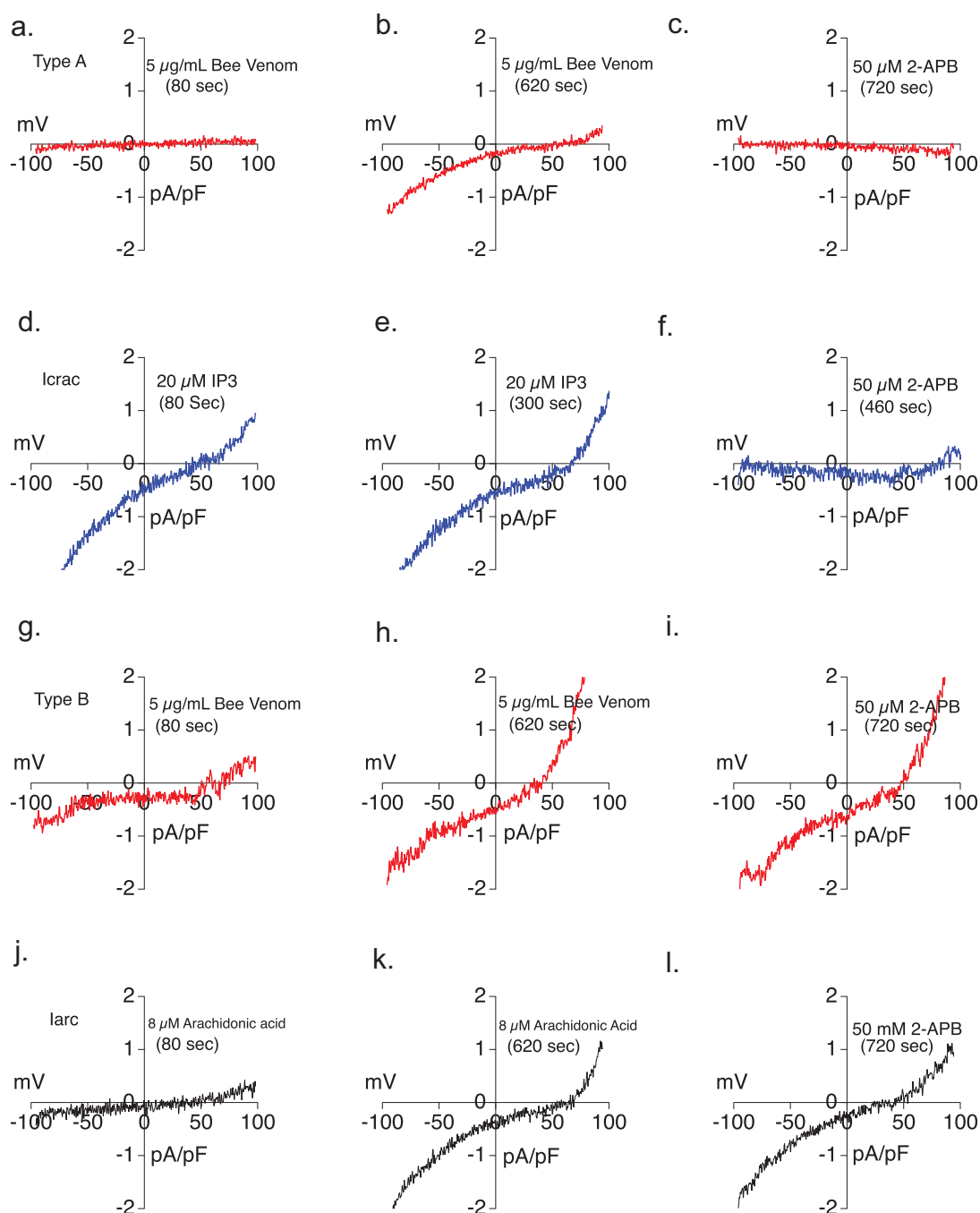


**Figure 3.** Attribution of CRAC- and Arc-like bee venom-induced currents using responsiveness to 2-APB. (a) Type A current-voltage relationship taken after background subtraction at 80 s of 5  $\mu\text{g}/\text{ml}$  bee venom application. The data in Figure 3(a–c) were all recorded from the same RBL2H3 cell over time. (b) Type A current-voltage relationship taken after background subtraction at 620 s of recording and 600 s of 5  $\mu\text{g}/\text{ml}$  bee venom application. (c) Current-voltage relationship recorded after background subtraction at 720 s of recording and 100 s of 50  $\mu\text{M}$  2-APB application to fully developed type A bee venom current. (d)  $I_{\text{crac}}$  current-voltage relationship taken after background subtraction at 80 s of 20  $\mu\text{M}$   $\text{IP}_3$  internal perfusion. The data in Figure 3(d,e,f) were all recorded from the same RBL2H3 cell ( $N = 5$ ). (e)  $I_{\text{crac}}$  current-voltage relationship taken after background subtraction at 300 s of 20  $\mu\text{M}$   $\text{IP}_3$  internal perfusion. (f) Current-voltage relationship recorded after background subtraction at 460 s of recording with 100 s of 50  $\mu\text{M}$  2-APB application to fully developed  $I_{\text{crac}}$  current. (g) Type B current-voltage relationship taken after background subtraction at 80 s of 5  $\mu\text{g}/\text{ml}$  bee venom application. The data in Figure 3 G, H and I were all recorded from the same RBL2H3 cell. (h) Type B current-voltage relationship taken after background subtraction at 620 s of recording and 600 s of 5  $\mu\text{g}/\text{ml}$  bee venom application. (i) Current-voltage relationship recorded after background subtraction at 720 s of recording and 100 s of 50  $\mu\text{M}$  2-APB application to fully developed type B bee venom current. (j)  $I_{\text{arc}}$  current-voltage relationship taken after background subtraction at 80 s of 8  $\mu\text{M}$  Arachidonic acid external application. The data in Figure 3(j,k,l) were all recorded from the same RBL2H3 cell ( $N = 4$ ). (k)  $I_{\text{ARC}}$  current-voltage relationship taken after background subtraction at 620 s of recording and 600 s of 8  $\mu\text{M}$  Arachidonic acid external application. (l) Current-voltage relationship recorded after background subtraction at 720 s of recording and 100 s of 50  $\mu\text{M}$  2-APB application to fully developed  $I_{\text{ARC}}$  current.

rectifying current with  $\sim +70$  mV reverse potential and sensitivity to 2-APB (Figure 3(d,e,f)). The arachidonic acid-induced ARC current also showed  $\sim +70$  mV reverse potential and inward rectification. ARC was resistant to 2-APB inhibition (Figure 3(j,k,l)) but could be inhibited by the trivalent ion Lanthanum ( $\text{La}^{3+}$ ) (data not shown)

The type C current resembles a non-selective cation current of the TRP family. In Figure 4 we tested the hypothesis that the Type C current could be TRPV1. This hypothesis was based on the fact that one prior study in sensory neurons suggested that TRPV1 could be activated by the BV component Mellitin [23]. We first compared this current to TRPV1 and then applied a known TRPV1 inhibitor to the Bee venom-induced Type C current. HEK293 cells overexpressing TRPV1 (HEK V1) were used to investigate if bee venom can activate TRPV1. Figure 4 shows a validation of this experimental system. First, 10  $\mu\text{M}$  Capsaicin, a TRPV1 agonist, was applied to wild-type HEK293 and HEKV1 cells as a control. Figure 4 (a) shows that capsaicin-induced calcium responses are present in HEK expressing TRPV1 but not wild-type cells, validating the system. Similarly, Figure 4(b,c) show that capsaicin-induced conductances are present in HEK expressing TRPV1 but not wild-type cells. Figure 4(d,e) show that the BV-induced conductance develops in HEK-TRPV1 but not WT HEK. At the 5  $\mu\text{g}/\text{ml}$  dose of BV, there is a long lag phase in the current development (Figure 4(e)), but at higher doses the current develops along a similar time course to that with Capsaicin (Figure 4(f,g)).

While initial TRPV1 currents are outwardly rectifying, these currents rapidly linearize to a non-rectified conductance and can be inactivated by washout (Figure 4(f,h)). These data are consistent with the established two state nature (normal and pore-dilated) of TRPV1 [33,34]. Figure 4(i-l) examines the dilation state of BV-induced TRPV1. As for Capsaicin, the BV-induced current rapidly linearizes and decreases in rectification. Low doses of BV can distinguish these two states but higher doses cannot. This is further evidenced in Figure 4(k), which shows that the conductance induced by BV is equally permeant to sodium and the large cation NMDG (N-methyl D-Glucamine). Permeation by NMDG is a hallmark of the dilated state of TRPV1 [35,36].

In WT cells (Figure 4(d)) a very small conductance was evoked by bee venom. We initially assumed this would represent the very small CRAC current that is present in HEK, but the extracted I/V curve (Figure 4(m,n)) is inconsistent with CRAC and may hint at a non-TRPV1 TRPV-family member such as TRPV2. We and others have exhaustively demonstrated that there is no endogenous TRPV1 in HEK (measured by response to Capsaicin), and indeed the extracted I/V in the HEK-TRPV1 does show a different rectification profile to that in the WT cells (Figure 4(m,n)).

We noted linearization of the I/V curve in response to bee venom (Figure 4(i,j)), and postulated that might represent either an attainment of the pore-dilated state of TRPV1 or that bee venom is initiating a different type of conductance at later time points due to some hemolytic activity (note though that cell viability remains high throughout the measurement period). We, therefore, applied a TRPV1 inhibitor to differentiate between these possibilities. Capsazepine was applied to Capsaicin-activated current, as a positive control, in the HEK-TRPV1 cells and the current decreased (Figure 5(a,b)). When applied to bee venom-elicited currents prior to any state transition or linearization, capsazepine caused a significant decrease in the current amplitude (Figure 5(c,d)). In contrast, when applied after the state transition or linearization has occurred (Figure 5(e,f)), capsazepine was without effect on the current amplitude. Overall, we observe both state 1 (non-dilated) and state 2 (pore-dilated) TRPV1 currents in response to BV, but also note a third manifestation in some cells where a very late developing large amplitude V1 (or possibly leak, not shown) appears that is also insensitive to the TRPV1 antagonist capsazepine.

### **Individual venom component mimetics activate different conductances in model mast cells**

The calcium assay data above suggest that several individual components that are found in the venom can cause calcium entry. We, therefore, explored whether the observed conductances in response to the whole venom could reflect conductances induced by individual components.

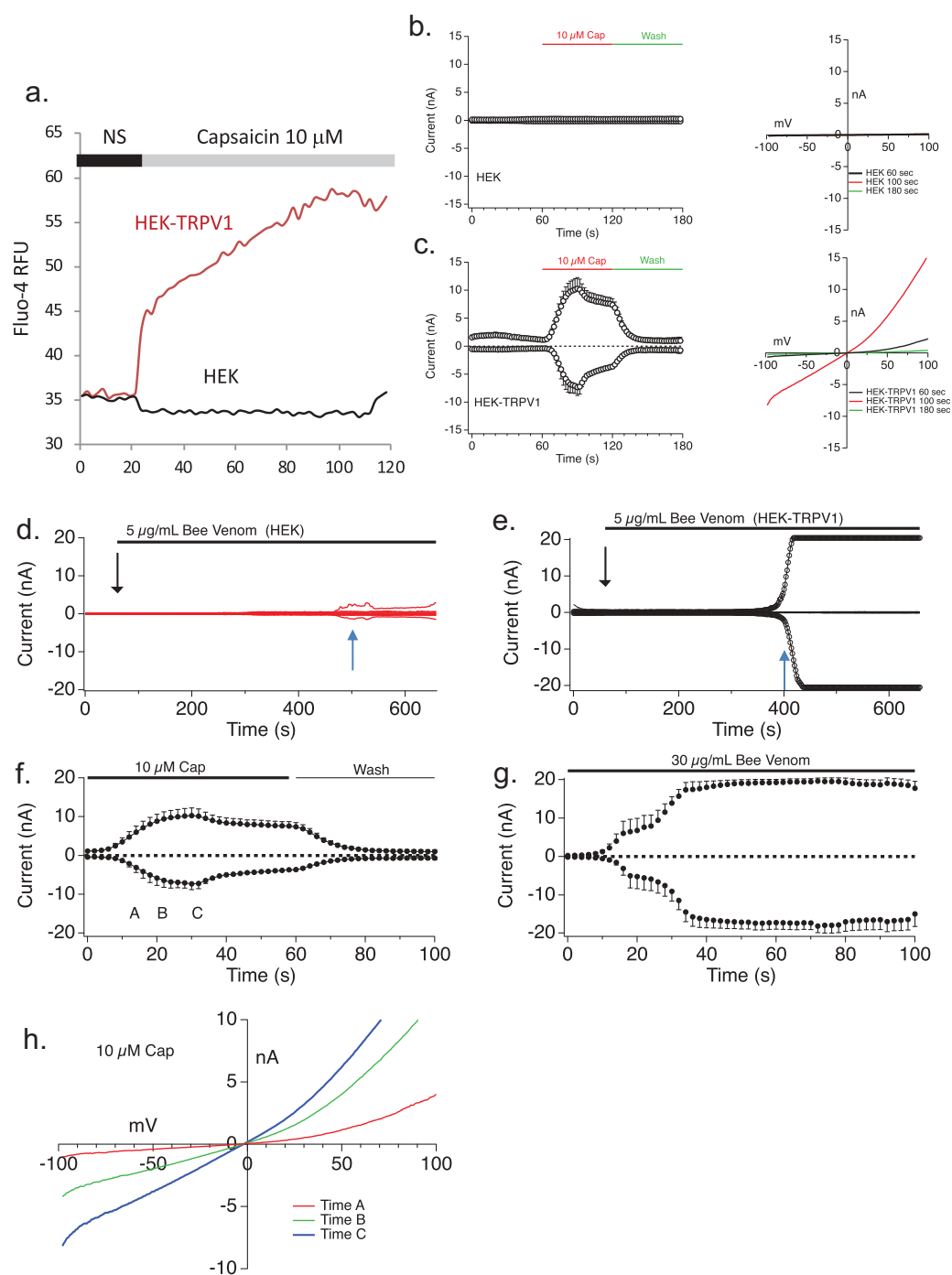


**Figure 4.** Relationship between TRPV1 and Bee Venom-induced currents. (a) HEK wild-type cells and TRPV1 overexpressing HEK cells were loaded with Fluo-4 and stimulated with capsaicin in the presence of 1mM external  $\text{CaCl}_2$ , showing TRPV1-dependent  $\text{Ca}^{2+}$  responses conferred by expression of the channel. (b,c) Capsaicin-induced conductance measurements in HEK (b) and HEK-TRPV1 (c). *Left panels* show current development over time. *Right panels* show current–voltage relationships. (d) Current development of HEK wild-type cells measured for 650 s with 600 s of 5  $\mu\text{g}/\text{mL}$  Bee Venom external application ( $n = 5$ ). (e) Current development of TRPV1 overexpressing HEK cells measured for 650 s with 600 s of 5  $\mu\text{g}/\text{mL}$  bee venom external application ( $n = 4$ ). Black downward arrows in D, E represent time of addition of stimulus. Blue upward arrows indicate time of extraction of I/V relationship shown in Figure 4(m,n,f). Current development of TRPV1 overexpressing HEK cells measured for 650 s with 600 s of 10 $\mu\text{M}$  Capsaicin external application ( $n = 4$ ). (g) Current development of TRPV1 overexpressing HEK cells measured for 650 s with 600 s of 30  $\mu\text{g}/\text{mL}$  bee venom external application ( $n = 4$ ). The current development graphs were generated by extracting currents at  $-80$  mV and  $+80$  mV. (h) Current–voltage relationship for TRPV1 stimulated by capsaicin. I/V curves were extracted at indicated time points in Figure 4(f). (i,j) Current–voltage relationship for conductance stimulated by Bee Venom. Current development over time is shown in (i), and I/V curves (j) were extracted at indicated time points in Figure 4(f). (k,l) Current development (k) and I/V relationships (l) of Bee Venom-induced conductances in HEK TRPV1 with sodium ( $\text{Na}^+$ ) or N-methyl D Glucosamine (NMDG) as the primary current carrier in the external solution. The current development graphs were generated by extracting currents at  $-80$  mV and  $+80$  mV. (m,n) Extracted I/V curves from Figure 4 D, E at times indicated by blue upward arrows, showing a lack of CRAC-like rectification and  $E_{\text{rev}}$  in the small HEK-WT conductance.

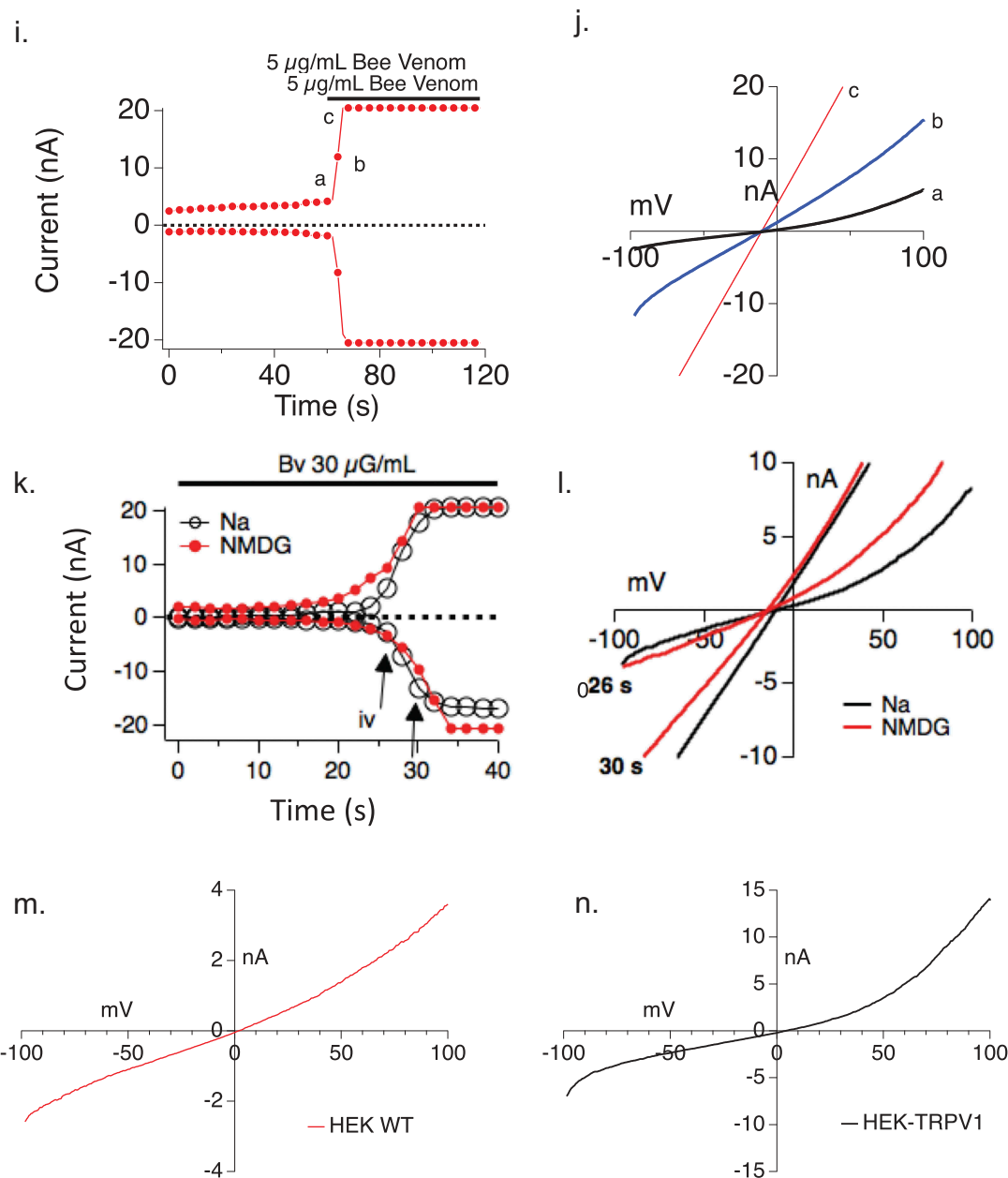
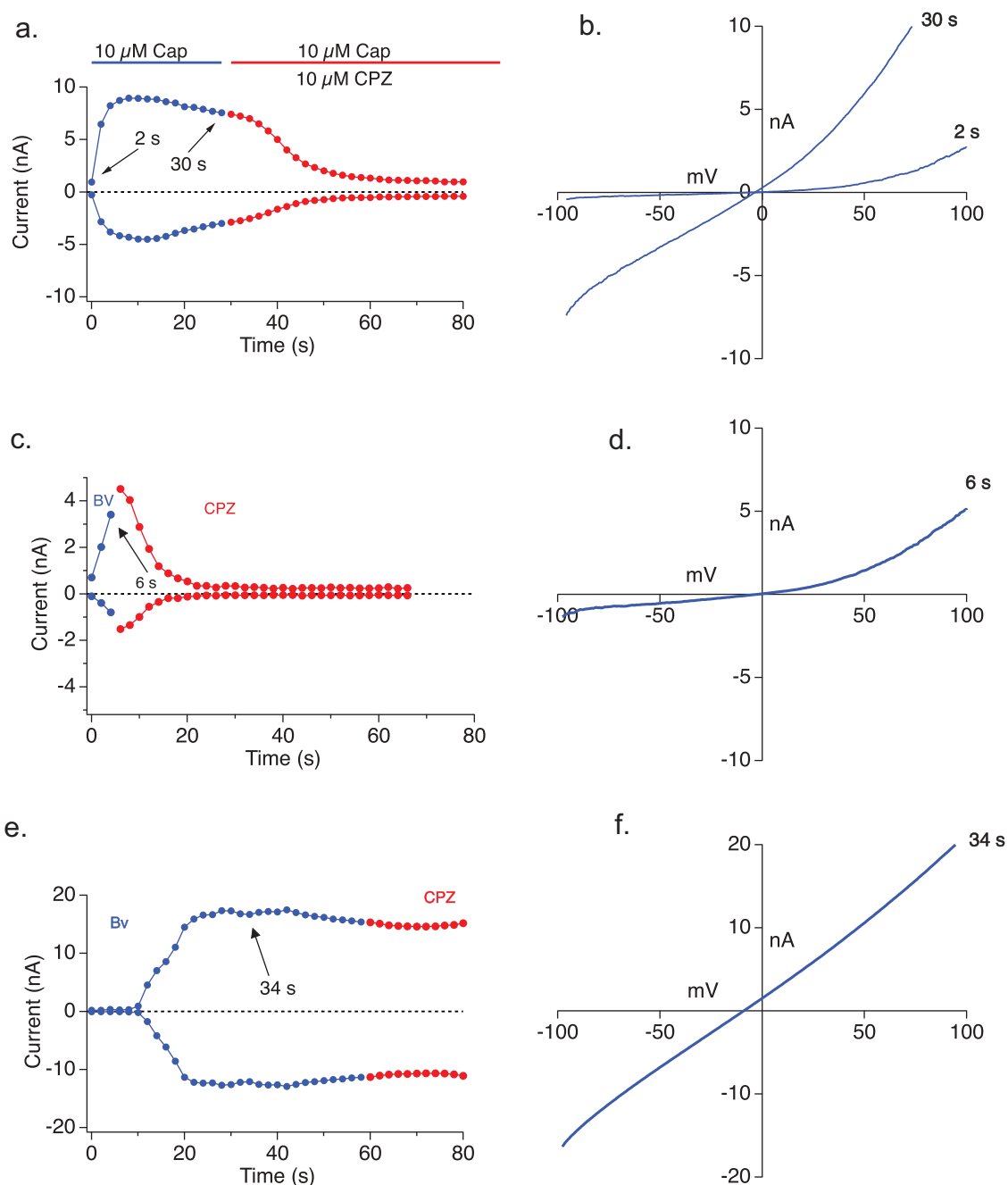


Figure 4. (Continued).

Antigenic cross-linking of Fc $\epsilon$ RI has been exhaustively shown to activate the CRAC current, which is not explored further here [37–40]. We focused upon Mastoparan, Arachidonic Acid, and Mellitin. In population-based Ca<sup>2+</sup> assays, Mastoparan elicited calcium influx (Figure 6(a)) but no appreciable store release in the bulk assay (Figure 6(b)), although at the single-cell level, we record a small percentage of cells that do manifest store release in response

to Mastoparan (not shown). Mastoparan was tested to see if it elicited a TRPV-like conductance and neither the I/V relationship nor the current development responses in HEK-TRPV1 challenged with Mastoparan support significant activity at TRPV1 (Figure 6(c)). In RBL2H3 cells we found that 10  $\mu\text{M}$  Mastoparan induced a CRAC-like current after leak subtraction that showed inward rectification with a reverse potential around +45 mV (Figure 6(c,d)). The



**Figure 5.** Bee Venom application elicits Capsazepine-sensitive and pore-dilating TRPV1 currents in TRPV1 over-expressing HEK cells. (a,b) Current development (a) and I/V relationship (b) of TRPV1 overexpressing HEK cells with 10  $\mu$ M Capsaicin application (blue) and followed by 10  $\mu$ M Capsazepine application (red) ( $n = 3$ ). (c,d) Current development (c) and I/V relationship (d) of TRPV1 overexpressing HEK cells after 30  $\mu$ g/ml bee venom application (blue) and 10  $\mu$ M Capsazepine application (red) with the TRPV1 inhibitor added at 10 sec. (e,f) Current development (e) and I/V relationship (f) of TRPV1 overexpressing HEK cells after 30  $\mu$ g/ml bee venom application (blue) and 10  $\mu$ M Capsazepine application (red) with the TRPV1 inhibitor added at 60 sec. The current development graphs were generated by extracting currents at  $-80$  mV and  $+80$  mV.

Mastoparan induced current in the RBL2H3 cells was sensitive to 50  $\mu$ M 2-APB and showed current inhibition similar to CRAC currents (Figure 6(d)). We noted that compound 48/80 (a synthetic secretagogue) also activated a CRAC-like

current, which was inhibited by 2-APB (data not shown).

Analysis of Mellitin, a bee venom component, revealed a complex picture. Mellitin (1  $\mu$ M) elicited calcium influx (Figure 7(a)) but no appreciable store

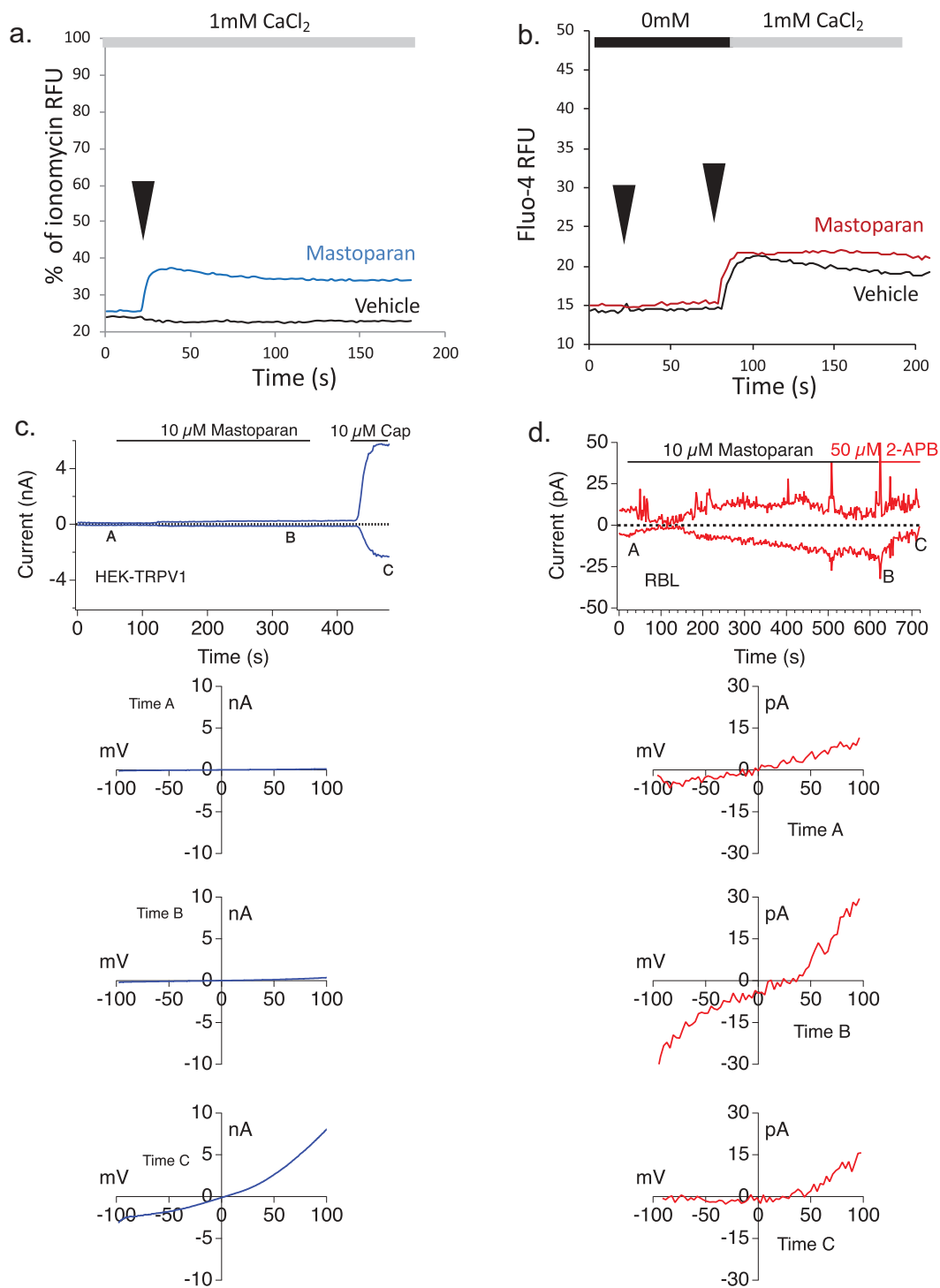


**Figure 6.** (a) Mastoparan application in RBL-2H3 and TRPV1 overexpression HEK cells (a) Fluo-4-AM was used to load RBL2H3 in a modified Ringer's solution containing 1 mM external CaCl<sub>2</sub>. Experimental readings were carried out either in 1mM external CaCl<sub>2</sub> (a) or in 0mM CaCl<sub>2</sub> with 1mM EGTA followed by readdition of CaCl<sub>2</sub> to a concentration of 1mM final. (B) Cells were stimulated after a period of establishing baseline (usually 20 s) by addition of vehicle (matched diluent to each stimulus), or 10 μM Mastoparan. Note that "vehicle" effect in B likely represents passive store depletion opening I<sub>CRAC</sub> channels rather than a Mastoparan effect. (c) *Upper panel.* Current development of a representative TRPV1 overexpressing HEK cell extracted at -80 mV and +80 mV over 480 s of recording after 300 s of 10 μM Mastoparan external application and 50 s of 10 μM Capsaicin application. *Lower panels.* Current-voltage relationships at indicated times in the current development from Figure 6(c). (d) *Upper panel.* Current development of a representative RBL2H3 cell extracted at -80 mV and +80 mV over 700 s of recording after 600 s of 10 μM Mastoparan external application and then application of 2-APB. *Lower panels.* Current-voltage relationships at indicated times in the current development from Figure 6(d). The current development graphs were generated by extracting currents at -80 mV and +80 mV.

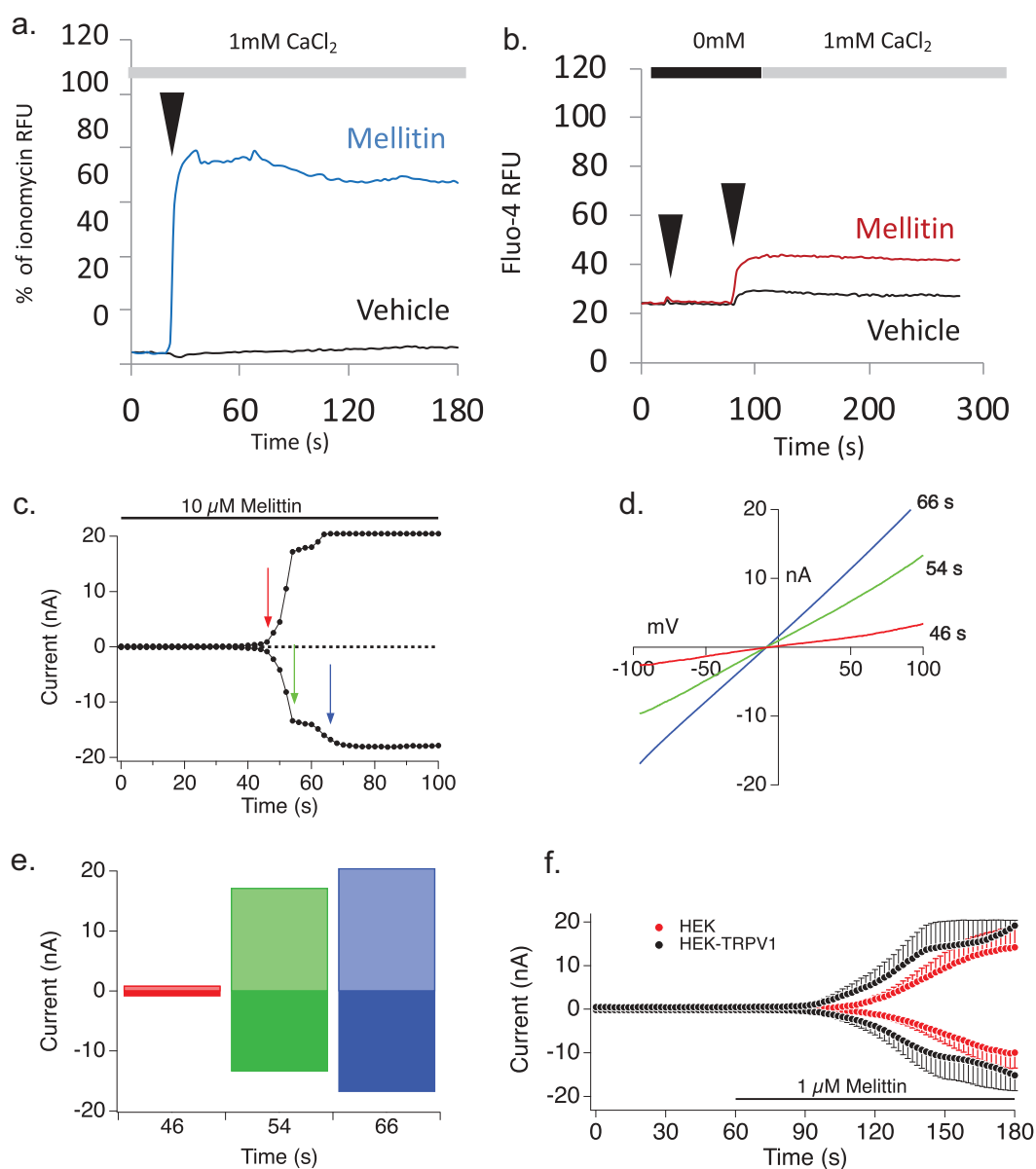


**Figure 7.** Melittin-induced Ca<sup>2+</sup> responses and conductances. (a,b) Fluo-4-AM was used to load RBL2H3 in a modified Ringer's solution containing 1 mM external CaCl<sub>2</sub>. Experimental readings were carried out either in 1mM external CaCl<sub>2</sub> (a) or in 0mM CaCl<sub>2</sub> with 1mM EGTA followed by re-addition of CaCl<sub>2</sub> to a concentration of 1mM final (b). Cells were stimulated after a period of establishing baseline (usually 20 s) by addition of vehicle (matched diluent to each stimulus), or 1 μM Mellitin. (c,d) Current development graph, extracted at -80 and +80 mV, (c) and I/V relationships (d) resulting from 10 μM Mellitin stimulation of RBL2H3. (e) Histogram representation of rectification characteristics of the conductances measured at the indicated time points in Figure 7(c,d). (f) Current development graph of HEK WT and HEK-TRPV1 stimulated with Mellitin. (g,h) Sensitivity of Mellitin-induced Ca<sup>2+</sup> responses to TRPV1 inhibitors in HEK-TRPV1. Fluo-4-AM was used to load RBL2H3 in a modified Ringer's solution containing 1 mM external CaCl<sub>2</sub>. Experimental readings were carried out in 1mM external CaCl<sub>2</sub>. Capsaicin (1 μM) (g) or Mellitin (10 μM) (h) were applied at 20 sec. After recording for a further 50 s, an inhibitor cocktail of 10 μM each of CPZ and BCTC was added. I, J. Sensitivity of Mellitin-induced Ca<sup>2+</sup> responses to TRPV1 inhibitors in RBL2H3. Fluo-4-AM was used to load RBL2H3 in a modified Ringer's solution containing 1 mM external CaCl<sub>2</sub>. Experimental readings were carried out in 1mM external CaCl<sub>2</sub>. Application sequences were Mellitin (20 s), followed by vehicle or an inhibitor cocktail of 10 μM each of CPZ and BCTC (40 s) (i), or vehicle followed by vehicle or the inhibitor cocktail (j). (k) Baseline (10 s timepoint), peak (25 s timepoint) or final attained (180 s timepoint) levels of Ca<sup>2+</sup> signal were plotted for RBL2H3 treated with Mellitin (at 20 s) then vehicle (at 60 s), blue bars; Mellitin (at 20 s) then CPZ/BCTC (at 60 s), red bars; or vehicle (at 20 s) then CPZ/BCTC (at 60 s), green bars.

release (Figure 7(b)) in RBL2H3. Melittin-induced currents in RBL2H3 are TRPV-like (Figure 7(c)) rather than CRAC- or ARC-like in their I/V

relationship (Figure 7(d)), and there has been a published study in sensory neurons suggesting Melittin activation of TRPV1 [41]. However, these

current rapidly lose their slight rectification (Figure 7(d,e)), and they could represent a pore-forming activity of Mellitin itself which would presumably manifest as a high  $I_{\max}$ , with a highly linear I/V, conductance [42,43]. Figure 7(f) shows that Mellitin is active both in HEK WT and TRPV1-expressing cells, suggesting that much of its activity is not dependent on the presence of TRPV1 protein. However, there is a slight difference between WT and TRPV1-expressing cells, in that current appears earlier in the TRPV1 containing cells and attains a slightly higher  $I_{\max}$  more rapidly (Figure 7(f)). We asked if inhibition of TRPV1 had any impact on the  $\text{Ca}^{2+}$  responses initiated by Mellitin. In bulk calcium assays in HEK-TRPV1, we see Mellitin behave as a pore-former (note rapid decline in fluorescence likely implies leaching of  $\text{Ca}^{2+}$  dye). However, this pore-forming activity is partially sensitive to a cocktail of two different modality TRPV1 inhibitors, Capsazepine (CPZ) and BCTC (N-(4-tert-Butylphenyl)-4-(3-chloropyridin-2-yl) piperazine-1-carboxamide) (Figure 7(h)) which affect Capsaicin-induced responses as would be expected (Figure 7(g)). In mast cells, we see the third scenario. Here, we note that there is less pore-forming activity (evidence of rapid dye-leaching) in response to 10  $\mu\text{M}$  Mellitin (*cf* Figure 7(i,h)) no effect of CPZ/BCTC (Figure 7(i,j,k)). Thus in HEK TRPV1, the effect of Mellitin appears primarily pore-forming with some contribution from a CPZ/BCTC-sensitive TRPV1. In RBL2H3 the cells are more resistant to the pore-forming activity of Mellitin (perhaps an immunocyte adaptation) and CPZ/BCTC are not impacting the  $\text{Ca}^{2+}$  entry. There are also marked dose-dependent differences since at 1  $\mu\text{M}$  Mellitin neither HEK-TRPV1 or RBL2H3 show the dye-leaching that we think indicates pore-forming activity of Mellitin.

### **Spatial analysis of response frequencies in populations of cells exposed to venom or its components**

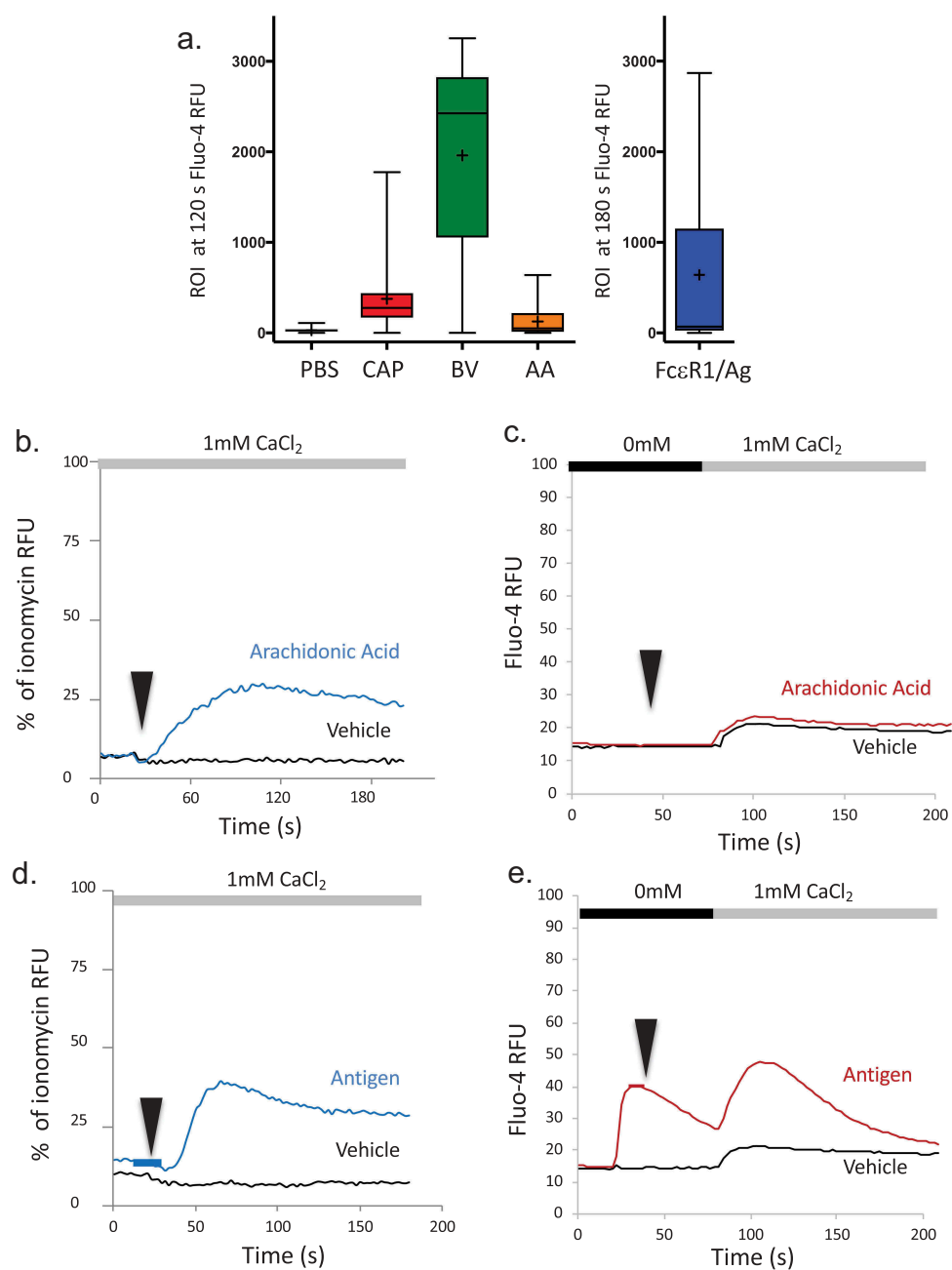
Population-based bulk calcium responses are recorded for  $\sim 300,000$  cells per datapoint. These types of data tell us little about the proportion of cells in a population that are responding and driving the bulk calcium signal. The current surveys and subsequent data, on the other hand, suggest that

single cells respond to Bee Venom in a differentiated fashion, i.e. one type of conductance predominates. We performed confocal imaging analysis of calcium signals across a population of RBL2H3. We examined fields of cells using confocal imaging of calcium fluxes and produced a frequency analysis of Fluo-4 fluorescence intensity at a 120-s benchmark timepoint, representing the sustained phase of a cell's calcium signaling response (Figure 8(a)). Regions of interest for each cell (ROI) were drawn at the interface with the coverslip in order to capture the area of the whole cell, and each cell's time series was averaged from 3 z discs at 25%, 50% and 75% of the cell's total height. Figure 8(a) summarizes the responses to the various stimuli and compares them to the population-based assays (Figures 8(b–e) and 2(a,b)). While responses to arachidonic acid are rarest, most cells respond to bee venom or secretagogue, and capsaicin and antigen/Fc $\epsilon$ RI are intermediate stimuli in terms of frequency of cell responses.

Using immunocytochemistry (Figure 9, Table 1), we could not find strong evidence of restricted channel expression (i.e. that individual cells expressed only one type of channel, CRAC, ARC or V1, for example). Certainly, many cells in populations of RBL2H3 co-stained positively with antibodies to two of the channels. These data suggest that the dominance of one conductance in a particular cell evidenced by the current survey in Figure 2 may not be explained simply by restricted expression of one channel type per cell. Figure 9(e) shows that, using confocal imaging, we looked at the impact of BCTC (TRPV1 inhibitor) and the CRAC inhibitor YM-58,483 on the population-based measured flux (area under the curve, AUC, of total cell population) and the number of cells contributing to that flux (% of the cells in the population that respond). There is a disconnect between these two measures, indicating that small numbers of cell can contribute disproportionately to measured population-based fluxes. These data also reinforce that inhibition of any one ion channel that is activated in response to BV may not be sufficient for therapeutic purposes.

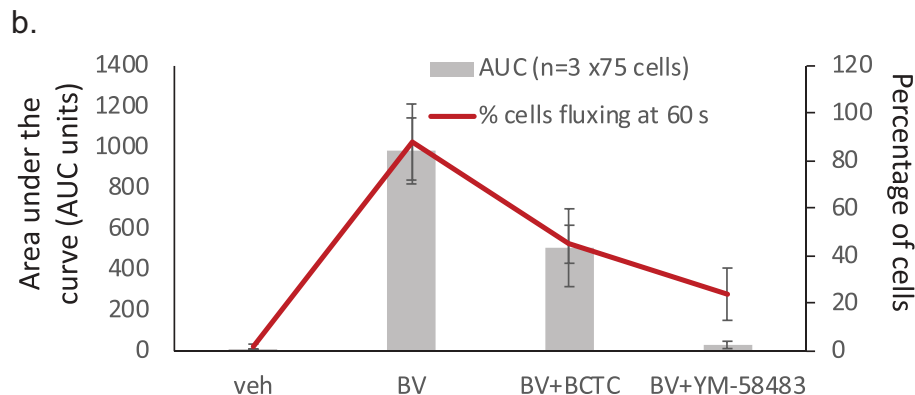
### **Summary**

Table II in Figure 10 offers a summary of the data presented in this study. Figure 10 summarizes the



**Figure 8.** Frequency of RBL2H3 activation by venom and related stimuli. (a) RBL2H3 were loaded with Fluo-4 and stimulated as indicated. Fields of cells were imaged using confocal imaging and regions of interest (ROI) were drawn (Nikon NIS Elements) around the circumference of each cell at a z layers positioned at 25%, 50%, and 75% of the measured height of the cell. Changes in Fluo-4 intensity over time were plotted for each ROI, averaged between the z discs, and a box plot generated for the minimum, maximum, median and 25th and 75th percentiles of attained fluorescence intensity in that ROI at 120 s (100 s after application of stimulus), or 180 s for FcεR1/antigen (also 100 s after application of stimulus). Numbers of ROI analyzed were PBS (n = 74), Capsaicin (n = 121), Bee venom (n = 160), Arachidonic acid (n = 74), FcεR1/antigen (n = 71). (b–e) Population-based responses to Arachidonic Acid, and FcεR1/antigen in the absence and presence of external Ca<sup>2+</sup>, shown in comparison to Figures 2(a,b); 6(a,b), and 7(a, b).

Stain	Percentage of cells staining positively (n=1000 cells)				
	Orai1	Orai3	TRPV1	TRPV2	TRPA1
Orai1	33				
Orai3	9	8			
TRPV1	38	6	55		
TRPV2	35	6	60	60	
TRPA1	5	0	18	45	17



**Figure 9.** Table 1 Frequency analysis of anti-ion channel immunofluorescence staining in RBL2H3. RBL2H3 were stained with the indicated antibodies alone or pairwise. After mounting, imaging was performed using epifluorescence and 1000 cells were scored for positive or negative membrane-localized staining for the indicated ion channel. Background subtraction was performed using instrument gains set on the basis of the secondary antibody alone control. Positive staining was defined as membrane positivity at 50% or greater of the maximal fluorescence signal for a given cell and color line. (b) Impact of TRPV1 and CRAC inhibitors on population-based calcium responses and frequency of those responses in RBL2H3.  $\text{Ca}^{2+}$  imaging was conducted as described for Figure 8 in the presence of vehicle, 30  $\mu\text{M}$  Bee Venom or 30  $\mu\text{M}$  Bee Venom with the addition of either 10  $\mu\text{M}$  BCTC or 10  $\mu\text{M}$  of the CRAC inhibitor YM-58,483. Area under the curve (AUC) or response frequency counts were then performed.

pathways initiated downstream of venom exposure identified in this study.

## Discussion

Mast cells respond to a strikingly diverse array of stimuli, ranging from immunological challenges, to environmental and physiological small molecules, to physicochemical and mechanical inputs. These stimuli may be experienced by the cell as single inputs, or in the context of complex mixtures such as venoms which contain multiple potentially activatory factors, or as co-incident inputs resulting from parallel simultaneous exposures. Ion channels, and especially calcium channels, are central examples of proteins that broker cellular responses to each of the stimulus categories above, and mast cells clearly co-express multiple calcium channels. A central question of

this paper was to begin decoding this complexity, asking how cells respond to complex stimuli at the single cell and population level, which channels are players in the responses, and what happens functionally and in terms of calcium signaling when co-incident stimuli are received that are capable of activating several signaling pathways in parallel. The key findings (see Table 2) of the current paper are (1) that bee venom contains components that activate multiple  $\text{Ca}^{2+}$ -permeant ion channels in mast cells including (but not limited to) TRPV, CRAC and ARC conductances, (2) that activation of these conductances can be attributed to specific venom components or their mimetics, and (3) that population-based measurements do not reflect the single-cell heterogeneity of responses, where application of the pluripotent stimuli to cells that co-express multiple ion channel species tends to

Table II.	Summary Table					
	Whole Venom	Arachidonic Acid	Mastoparan	Mellitin	C48/80	FcεRI
Primary current observed (% of cells)	I <sub>CRAC</sub> (50%) I <sub>ARC</sub> (33%) TRPV1 (17%)	I <sub>ARC</sub>	CRAC-like	TRPV1	CRAC-like	I <sub>CRAC</sub>
E <sub>rev</sub>	+70 mV (CRAC), +70 mV, (ARC), 0 mV (TRPV1)	+67 mV	+45 mV	0 mV	+22 mV	+65 mV
I max (inward current)	1.17 pA/pF (CRAC), 2.63 pA/pF, (ARC), 444 pA/pF (TRPV1)	1.95 pA/pF	1.06 pA/pF	20 nA	1 pA/pF	2.87 pA/pF
EC50 (Ca entry)	11 μg/ml	8 μM	10 μg/ml	3 μM	300 ng/ml	140 ng/ml
Store depletion initiated?	Yes	Yes	Yes	Yes	Yes	Yes
normalized AUC	1.0	0.03	0.6	0.2	0.2	0.8
AUC <i>p</i> value (compared to whole venom)	N/A	0.0005	0.005	0.005	0.005	0.01
Calcium influx initiated?	Yes	Yes	Yes	Yes	Yes	Yes
Secretory response initiated?						
RBL2H3	Yes	No	Yes	Yes	Yes	Yes
BMMC	Yes	No	Yes	No	No	Yes
Primary basophils	Yes	No	Yes	Yes	Yes	Yes

**Figure 10.** Table 2 Summary of data presented in this study. Tabulation of the primary-observed current, its physiological characteristics and downstream effects on calcium release, Ca<sup>2+</sup> entry and secretory responses, in response to the whole venom of the indicated components. (a) Schematic summary of putative venom-induced ionotropic pathways in mast cells. Both venom itself (via its intrinsic peptide and small-molecule secretagogue components) and the physicochemical changes in tissue that are initiated by envenomation have the potential to activate TRPV subfamily non-selective cation channels. Venom PLA2 can generate AA, which has the capacity to activate ARC, and there are well-established pathways for antigenic activation of the CRAC pathway. Possible additional linkages are denoted by pink arrows. GPCR, G-protein-coupled receptor; TRP, Transient Receptor Potential; AA, Arachidonic Acid; ARC, Arachidonic acid Activated current; SERCA, Sarcoplasmic-Endoplasmic Reticulum Ca<sup>2+</sup>-ATPase; Thaps, Thapsigargin; InsP3, inositol 1,4,5, trisphosphate; CRAC, Ca<sup>2+</sup>-Release Activated Current; ORA11, calcium selective ion channel encoded in humans by the ORA11 gene; FcεRI, high affinity receptor for immunoglobulin E; IgE, immunoglobulin E.

lead to the measurement of one dominant conductance per cell. The first and second observations have implications for therapeutic targeting of ion channels to suppress unwanted responses to venom and for the informed design of therapeutic *Hymenoptera*-based therapies [44–50] for cancer, pain, and inflammation. The third of these key

findings is intriguing and suggests a novel mechanism by which cellular decisions to activate one ion channel rather than another, despite co-expression, for future investigation.

We performed a current survey of a model mast cell line selected for its pleiotropic responsiveness to multiple pro-inflammatory inputs, the RBL2H3.

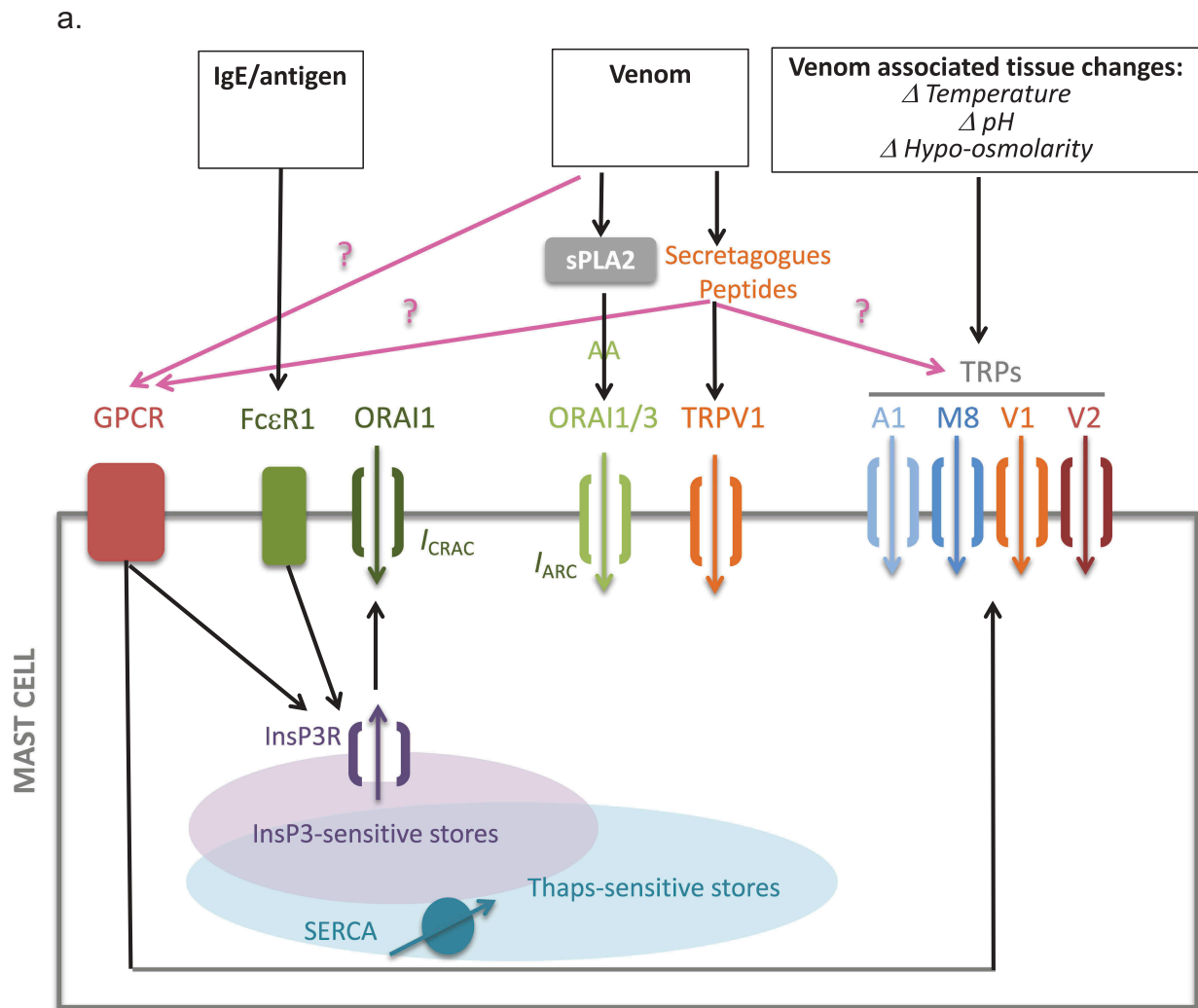


Figure 10. (Continued).

Future studies will need to replicate these experiments in cells such as peripheral blood basophils, since tissue-isolated primary mast cells may offer prohibitive technical challenges. We initially focused on only three calcium entry mechanisms, which significantly underestimates the true complexity of the system, since other TRPV, TRPA, TRPC, TRPM, and other calcium permeant conductances are likely to be present in this system [51–54]. Our data show that  $I_{CRAC}$ ,  $I_{ARC}$  and TRPV conductances are present in model mast cell populations, but at varying frequencies and abundancies, and responding to diverse single stimuli. Heterogeneous stimuli such as *Hymenoptera* venom may activate multiple classes of conductance at the population level but tend to lead to the measurement of only one type of conductance

per cell. Having identified interesting findings in this cell line, we will extend our findings to primary bone marrow-derived mast cells and human blood basophils. Preliminary data (not shown) from these studies suggest that the immature bone marrow-derived mast cells are more CRAC-dominant, whereas basophils have wider representations of ARC and TRP responses similar to RBL2H3. Limitations on our ability to isolate tissue-conditioned and resident mast cells make it difficult to assess whether the diversity of expression of conductances is related to maturation or conditioning of distinct mast cell subsets.

The responses to the whole venom suggest that in individual cells are programmed to respond primarily via one conductance pathway, despite the fact that with venom application they

are coincidentally experiencing stimuli that can target multiple conductances. Venom exposure results in the development of CRAC-like, ARC-like, and TRPV-like currents. Our immunofluorescence data suggest that this is not solely reflecting the differential expression of channel proteins, in that we see many cells that immunodecorated with antibodies against two or more of the channel species studied here. Thus, the mechanism by which one pathway gains dominance in cells that express the machinery for multiple responses is not yet clear but is likely to be complex since other factors such as cell cycle status can impact the representation of channel species in individual cells [55]. It seems likely that in this RBL2H3 system, the population has some pre-existing heterogeneity in either expression of the channels and/or their functionality. If translated to physiological mast cells *in vivo*, this heterogeneity might be reminiscent of the situation in sensory neuron bundles, where individual cells express different combinations of dominant TRPV-family channels to encode differential responses to physicochemical inputs [56,57].

Our study provides some in-depth analysis of responses to venom components or their mimetics. However, while we have studied exemplars of the main *classes* of likely ionotropic stimuli in the complex venom mixture, there may well remain additional stimuli that are coupled to  $\text{Ca}^{2+}$  entry (e.g. other secretagogue peptides, small molecules such as cyclin nucleotides, other bioactive lipids). We suggest that systematic venom dissection with fractionation coupled to higher throughput electrophysiology would be the next steps in evaluating these possibilities. The secretagogue mastoparan is stimulating broadly CRAC-like currents (highly positive reversal potentials, low amplitude, sensitivity to 2-APB). This is inconsistent with any lytic activity of mastoparan [58], which could result in large linear currents. Rather, in these cells a classic mastoparan mechanism is more likely, direct activation of Gq [59,60] or PLC [61,62] leading to Ins (1,4,5) P3 production and store release followed by CRAC activation [63,64]. In our bulk assays, we do not detect predicted calcium store release in response to mastoparan, possibly due to the sensitivity of the system.

The lack of ARC-like currents in response to mastoparan is consistent with the finding of Choi *et al.*, who found that mastoparan does not mobilize AA formation [65].

We also assessed compound 48/80, a mast cell secretagogue often studied in parallel to mastoparan. The currents that respond to compound 48/80 have a more TRP-like I/V curve, [66] and a lack of sensitivity to 2-APB (data not shown). We have not definitively identified them, and our practice of using close to physiological amounts of  $\text{Mg}^{2+}$  (1 mM compared to physiological levels of ~0.5 mM) in our recording solutions, rather than the high levels of  $\text{Mg}^{2+}$  needed to block TRPM7, may be leading to TRPM7 presence in these recordings and larger than actual outward currents as a result, so we did not include them in this report. Further work on both Mastoparan and other secretagogues may be of interest: A recent paper suggests that ORAI2 (a CRAC component) augments antigen- and secretagogue-induced calcium responses [37]. Older studies suggest that secretagogues can work via PLD [67], and the PLD product phosphatidic acid (PA) has been linked to potassium channels and TRPV1 (as lyso-PA) [68,69]. More complexity is suggested by a study showing that secretagogue-induced release and influx responses can be differentially reliant on AA signaling [70], and by possible G-protein involvement [71].

Mellitin is a venom component with interesting properties. Mellitin clearly activates TRPV1-dependent responses and has previously been shown to activate V1 in sensory neurons [23]. Mellitin poses several open questions. We have not yet discerned the difference between “pore-forming” activity and the ability to induce the dilated, highly permeant, state of TRPV1 or possibly the activation of TRPV2 or another TRP (given the lack of sensitivity to CPZ/BCTC). At low concentrations, Mellitin can also clearly induce some conductance in the WT HEK cells that do not appear to represent a lytic current, possibly this is TRPV2 or a TRPC conductance [72]. RBL2H3 show a linear TRPV-like current in response to mellitin, which compares closely to either pore-dilated V1 currents induced by mellitin in a TRPV1 over-expression system or to the type of conductance related to the putative pore-

forming role of some venom peptide components. Such pore-forming peptides can be lytic or non-lytic, and the apparent health of the cells (no obvious morphological changes, not trypan blue positive) under conditions of venom or mellitin application suggest that direct hemolysis is not occurring during our experimental time period.

In summary, heterogeneous stimuli such as *Hymenoptera* venom may activate multiple classes of conductance at the population level but at the single-cell level initiate single conductance responses that are heterogeneous across the cell lines used here, and appear to be similarly heterogeneous in single-cell calcium assays of primary basophils and mast cells (not shown). The mechanism by which the multi-component venom, at the single-cell level, is somehow “less than the sum of its parts” and selectively activates one conductance type per cell, is of interest to explore in future studies. The relationship between our data and prior studies showing “all or none” single cells responses but graded population responses via CRAC merit further study [40]. Single-cell secretion assays are also required to assess which venom-activated pathways are resulting in functional responses downstream of calcium entry, as not all calcium entry profiles seen here may be sufficient to initiate histamine secretion, for example. Identification of the molecular targets of Bee Venom within the diversity of  $\text{Ca}^{2+}$  channels, and the functional impact of the resulting  $\text{Ca}^{2+}$  entry, may inform decisions about which channels should be targeted to mitigate pathological effects of envenomation. Finally, in addition to the presumed mast cell activatory, pro-inflammatory, responses studied here, the implications of bee venom therapeutically as a desensitizing agent for a nociceptive TRP such as TRPV1 should be considered in the documented anti-inflammatory and anti-nociceptive effects of venom [47,73].

## Acknowledgments

The authors remember Carl Sung and acknowledge his contributions to this work. This work was funded by the Victoria and Bradley Geist Foundation (grants 45408 and 19CON-95456), the National Institutes of Health P20MD006084, the NIH R15 DK 100978, the NIH INBRE 2P20GM103466 (all HT) and the NIH COBRE P20GM113134 (AJS). KMU was funded by The Carlsberg Foundation.

## Disclosure statement

No potential conflict of interest was reported by the authors.

## Funding

This work was supported by the National Institutes of Health [P20MD006084]; National Institutes of Health [P20GM113134]; National Institutes of Health [P20GM103466]; National Institutes of Health [R15 DK 100978]; The Carlsberg Foundation [NA]; Victoria S. and Bradley L. Geist Foundation [19 CON 95456]; Victoria S. and Bradley L. Geist Foundation [45408].

## ORCID

A.J. Stokes  <http://orcid.org/0000-0002-3526-4685>

## References

- [1] Munaron L. Shuffling the cards in signal transduction: calcium, arachidonic acid and mechanosensitivity. *World J Biol Chem.* 2011;2:59–66.
- [2] Prussin C, Metcalfe DD. 4. IgE, mast cells, basophils, and eosinophils. *J Allergy Clin Immunol.* 2003;111: S486–94.
- [3] Wischmeyer E, Lentz KU, Karschin A. Physiological and molecular characterization of an IRK-type inward rectifier  $\text{K}^+$  channel in a tumour mast cell line. *Pflugers Arch.* 1995;429:809–819.
- [4] Bradding P, Okayama Y, Kambe N, et al. Ion channel gene expression in human lung, skin, and cord blood-derived mast cells. *J Leukoc Biol.* 2003;73:614–620.
- [5] Serhan CN, Ward PA, Gilroy DW. *Fundamentals of inflammation.* Cambridge; New York: Cambridge University Press; 2010.
- [6] Son DJ, Lee JW, Lee YH, et al. Therapeutic application of anti-arthritis, pain-releasing, and anti-cancer effects of bee venom and its constituent compounds. *Pharmacol Ther.* 2007;115:246–270.
- [7] Zhang S, Liu Y, Ye Y, et al. Bee venom therapy: potential mechanisms and therapeutic applications. *Toxicol.* 2018;148:64–73.
- [8] Wajdner HE, Farrington J, Barnard C, et al. Orai and TRPC channel characterization in FcepsilonRI-mediated calcium signaling and mediator secretion in human mast cells. *Physiol Rep.* 2017;5: pii: e13166.
- [9] Barnhill JC, Stokes AJ, Koblan-Huberson M, et al. RGA protein associates with a TRPV ion channel during biosynthesis and trafficking. *J Cell Biochem.* 2004;91:808–820.
- [10] Stokes AJ, Shimoda LM, Koblan-Huberson M, et al. A TRPV2-PKA signaling module for transduction of

- physical stimuli in mast cells. *J Exp Med.* 2004;200:137–147.
- [11] Stokes AJ, Wakano C, Del Carmen KA, et al. Formation of a physiological complex between TRPV2 and RGA protein promotes cell surface expression of TRPV2. *J Cell Biochem.* 2005;94:669–683.
- [12] Smith PK, Nilius B. Transient receptor potentials (TRPs) and anaphylaxis. *Curr Allergy Asthma Rep.* 2013;13:93–100.
- [13] Hoth M, Penner R. Depletion of intracellular calcium stores activates a calcium current in mast cells. *Nature.* 1992;355:353–356.
- [14] Hou X, Pedi L, Diver MM, et al. Crystal structure of the calcium release-activated calcium channel Orai. *Science.* 2012;338:1308–1313.
- [15] Yen M, Lewis RS. Numbers count: how STIM and Orai stoichiometry affect store-operated calcium entry. *Cell Calcium.* 2019;79:35–43.
- [16] Hoth M, Penner R. Calcium release-activated calcium current in rat mast cells. *J Physiol.* 1993;465:359–386.
- [17] Zhang SL, Yu Y, Roos J, et al. STIM1 is a Ca<sup>2+</sup> sensor that activates CRAC channels and migrates from the Ca<sup>2+</sup> store to the plasma membrane. *Nature.* 2005;437:902–905.
- [18] Liou J, Kim ML, Heo WD, et al. STIM is a Ca<sup>2+</sup> sensor essential for Ca<sup>2+</sup>-store-depletion-triggered Ca<sup>2+</sup> influx. *Curr Biol.* 2005;15:1235–1241.
- [19] Raisinghani M, Pabbidi RM, Premkumar LS. Activation of transient receptor potential vanilloid 1 (TRPV1) by resiniferatoxin. *J Physiol.* 2005;567:771–786.
- [20] Ross RA. Anandamide and vanilloid TRPV1 receptors. *Br J Pharmacol.* 2003;140:790–801.
- [21] Raghuraman H, Chattopadhyay A. Melittin: a membrane-active peptide with diverse functions. *Biosci Rep.* 2007;27:189–223.
- [22] Argiolas A, Pisano JJ. Facilitation of phospholipase A2 activity by mastoparans, a new class of mast cell degranulating peptides from wasp venom. *J Biol Chem.* 1983;258:13697–13702.
- [23] Du YR, Xiao Y, Lu ZM, et al. Melittin activates TRPV1 receptors in primary nociceptive sensory neurons via the phospholipase A2 cascade pathways. *Biochem Biophys Res Commun.* 2011;408:32–37.
- [24] Chen J, Guan SM, Sun W, et al. Melittin, the major pain-producing substance of bee venom. *Neurosci Bull.* 2016;32:265–272.
- [25] Samways DS, Egan TM. Calcium-dependent decrease in the single-channel conductance of TRPV1. *Pflugers Arch.* 2011;462:681–691.
- [26] Hardie RC, Muallem S. Lipids in Ca<sup>2+</sup> signalling—an introduction. *Cell Calcium.* 2009;45:517–520.
- [27] Meves H. Arachidonic acid and ion channels: an update. *Br J Pharmacol.* 2008;155:4–16.
- [28] Thompson JL, Mignen O, Shuttleworth TJ. The ARC channel—an endogenous store-independent Orai channel. *Curr Top Membr.* 2013;71:125–148.
- [29] Shuttleworth TJ. Arachidonic acid, ARC channels, and Orai proteins. *Cell Calcium.* 2009;45:602–610.
- [30] Lee JA, Son MJ, Choi J, et al. Bee venom acupuncture for rheumatoid arthritis: a systematic review of randomised clinical trials. *BMJ Open.* 2014;4:e006140.
- [31] Passante E, Frankish N. The RBL-2H3 cell line: its provenance and suitability as a model for the mast cell. *Inflamm Res.* 2009;58:737–745.
- [32] Paredes RM, Etzler JC, Watts LT, et al. Chemical calcium indicators. *Methods.* 2008;46:143–151.
- [33] Cao E, Liao M, Cheng Y, et al. TRPV1 structures in distinct conformations reveal activation mechanisms. *Nature.* 2013;504:113–118.
- [34] Chung MK, Guler AD, Caterina MJ. TRPV1 shows dynamic ionic selectivity during agonist stimulation. *Nat Neurosci.* 2008;11:555–564.
- [35] Jansson ET, Trkulja CL, Ahemaiti A, et al. Effect of cholesterol depletion on the pore dilation of TRPV1. *Mol Pain.* 2013;9:1.
- [36] Munns CH, Chung MK, Sanchez YE, et al. Role of the outer pore domain in transient receptor potential vanilloid 1 dynamic permeability to large cations. *J Biol Chem.* 2015;290:5707–5724.
- [37] Tsvilovskyy V, Solis-Lopez A, Schumacher D, et al. Deletion of Orai2 augments endogenous CRAC currents and degranulation in mast cells leading to enhanced anaphylaxis. *Cell Calcium.* 2018;71:24–33.
- [38] Ng SW, Di Capite J, Singaravelu K, et al. Sustained activation of the tyrosine kinase Syk by antigen in mast cells requires local Ca<sup>2+</sup> influx through Ca<sup>2+</sup>-release-activated Ca<sup>2+</sup> channels. *J Biol Chem.* 2008;283:31348–31355.
- [39] Di Capite JL, Bates GJ, Parekh AB. Mast cell CRAC channel as a novel therapeutic target in allergy. *Curr Opin Allergy Clin Immunol.* 2011;11:33–38.
- [40] Chang WC, Di Capite J, Nelson C, et al. All-or-none activation of CRAC channels by agonist elicits graded responses in populations of mast cells. *J Immunol.* 2007;179:5255–5263.
- [41] Li MM, Yu YQ, Fu H, et al. Extracellular signal-regulated kinases mediate melittin-induced hypersensitivity of spinal neurons to chemical and thermal but not mechanical stimuli. *Brain Res Bull.* 2008;77:227–232.
- [42] Gimenez D, Sanchez-Munoz OL, Salgado J. Direct observation of nanometer-scale pores of melittin in supported lipid monolayers. *Langmuir.* 2015;31:3146–3158.
- [43] Krauson AJ, He J, Wimley WC. Determining the mechanism of membrane permeabilizing peptides: identification of potent, equilibrium pore-formers. *Biochim Biophys Acta.* 2012;1818:1625–1632.
- [44] Rady I, Siddiqui IA, Rady M, et al. Melittin, a major peptide component of bee venom, and its conjugates in cancer therapy. *Cancer Lett.* 2017;402:16–31.
- [45] Lee WR, Pak SC, Park KK. The protective effect of bee venom on fibrosis causing inflammatory diseases. *Toxins (Basel).* 2015;7:4758–4772.

- [46] Ye X, Guan S, Liu J, et al. Activities of venom proteins and peptides with possible therapeutic applications from bees and WASPS. *Protein Pept Lett.* **2016**;23:748–755.
- [47] Lee G, Bae H. Anti-inflammatory applications of melittin, a major component of bee venom: detailed mechanism of action and adverse effects. *Molecules.* **2016**;21:616.
- [48] Lee SH, Lee JM, Kim YH, et al. Antialloodynic effects of bee venom in an animal model of complex regional pain syndrome type 1 (CRPS-I). *Toxins (Basel).* **2017**;9:285.
- [49] Choi J, Jeon C, Lee JH, et al. Suppressive effects of bee venom acupuncture on paclitaxel-induced neuropathic pain in rats: mediation by spinal alpha(2)-adrenergic receptor. *Toxins (Basel).* **2017**;9.
- [50] Uzair B, Bushra R, Khan BA, et al. Potential uses of venom proteins in treatment of HIV. *Protein Pept Lett.* **2018**;25:619–625.
- [51] Ashmole I, Bradding P. Ion channels regulating mast cell biology. *Clin Exp Allergy.* **2013**;43:491–502.
- [52] Stokes A, Wakano C, Koblan-Huberson M, et al. TRPA1 is a substrate for de-ubiquitination by the tumor suppressor CYLD. *Cell Signal.* **2006**;18:1584–1594.
- [53] Huang L, Ng NM, Chen M, et al. Inhibition of TRPM7 channels reduces degranulation and release of cytokines in rat bone marrow-derived mast cells. *Int J Mol Sci.* **2014**;15:11817–11831.
- [54] Freichel M, Almering J, Tsvilovskyy V. The role of TRP proteins in mast cells. *Front Immunol.* **2012**;3:150.
- [55] Tani D, Monteilh-Zoller MK, Fleig A, et al. Cell cycle-dependent regulation of store-operated I(CRAC) and Mg<sup>2+</sup>-nucleotide-regulated MagNuM (TRPM7) currents. *Cell Calcium.* **2007**;41:249–260.
- [56] Vandewauw I, De Clercq K, Mulier M, et al. A TRP channel trio mediates acute noxious heat sensing. *Nature.* **2018**;555:662–666.
- [57] Julius D. TRP channels and pain. *Annu Rev Cell Dev Biol.* **2013**;29:355–384.
- [58] Cabrera MP, Alvares DS, Leite NB, et al. New insight into the mechanism of action of wasp mastoparan peptides: lytic activity and clustering observed with giant vesicles. *Langmuir.* **2011**;27:10805–10813.
- [59] Higashijima T, Uzu S, Nakajima T, et al. Mastoparan, a peptide toxin from wasp venom, mimics receptors by activating GTP-binding regulatory proteins (G proteins). *J Biol Chem.* **1988**;263:6491–6494.
- [60] Yajima Y, Uchino K, Ito H, et al. Mastoparan-stimulated prolactin secretion in rat pituitary GH3 cells involves activation of Gq/11 proteins. *Endocrinology.* **1997**;138:1949–1958.
- [61] Schnabel P, Gas H, Nohr T, et al. G protein-independent stimulation of human myocardial phospholipase C by mastoparan. *Br J Pharmacol.* **1997**;122:31–36.
- [62] Wallace MA, Carter HR. Effects of the wasp venom peptide, mastoparan, on a phosphoinositide-specific phospholipase C purified from rabbit brain membranes. *Biochim Biophys Acta.* **1989**;1006:311–316.
- [63] Hirata Y, Atsumi M, Ohizumi Y, et al. Mastoparan binds to glycogen phosphorylase to regulate sarcoplasmic reticular Ca<sup>2+</sup> release in skeletal muscle. *Biochem J.* **2003**;371:81–88.
- [64] Lin SZ, Yan GM, Koch KE, et al. Mastoparan-induced apoptosis of cultured cerebellar granule neurons is initiated by calcium release from intracellular stores. *Brain Res.* **1997**;771:184–195.
- [65] Choi OH, Padgett WL, Daly JW. Effects of the amphiphilic peptides melittin and mastoparan on calcium influx, phosphoinositide breakdown and arachidonic acid release in rat pheochromocytoma PC12 cells. *J Pharmacol Exp Ther.* **1992**;260:369–375.
- [66] Kuno M, Okada T, Shibata T. A patch-clamp study: secretagogue-induced currents in rat peritoneal mast cells. *Am J Physiol.* **1989**;256:C560–8.
- [67] Chahdi A, Fraundorfer PF, Beaven MA. Compound 48/80 activates mast cell phospholipase D via heterotrimeric GTP-binding proteins. *J Pharmacol Exp Ther.* **2000**;292:122–130.
- [68] Raja M. The role of phosphatidic acid and cardiolipin in stability of the tetrameric assembly of potassium channel KcsA. *J Membr Biol.* **2010**;234:235–240.
- [69] Morales-Lazaro SL, Rosenbaum T. A painful link between the TRPV1 channel and lysophosphatidic acid. *Life Sci.* **2015**;125:15–24.
- [70] Kuno M, Kawawaki J, Shibata T, et al. Inhibitors of the arachidonic acid cascade dissociate 48/80-induced Ca<sup>2+</sup> influx and Ca<sup>2+</sup> release in mast cells. *Am J Physiol.* **1993**;264:C912–7.
- [71] Kuno M, Kawaguchi J, Mukai M, et al. PT pretreatment inhibits 48/80-induced activation of Ca(+)-permeable channels in rat peritoneal mast cells. *Am J Physiol.* **1990**;259:C715–22.
- [72] Ding J, Zhang JR, Wang Y, et al. Effects of a non-selective TRPC channel blocker, SKF-96365, on melittin-induced spontaneous persistent nociception and inflammatory pain hypersensitivity. *Neurosci Bull.* **2012**;28:173–181.
- [73] Marti MC, Stancombe MA, Webb AA. Cell- and stimulus type-specific intracellular free Ca<sup>2+</sup> signals in Arabidopsis. *Plant Physiol.* **2013**;163:625–634.